IOP Publishing | International Atomic Energy Agency Nuclear Fusion

Nucl. Fusion **62** (2022) 086010 (23pp) https://doi.org/10.1088/1741-4326/ac6ef2

Implementation of a Kalman filter-based eddy current estimator for the P-EFIT magnetic equilibrium reconstruction code

Yao Huang[1,a], Adriano Mele[2,a,*], Zhengping Luo[1], Massimiliano Mattei[3,4], Alfredo Pironti[3,4], Bingjia Xiao[1] and Qiping Yuan[1]

[1] Institute of Plasma Physics, Chinese Academy of Sciences, 350 Shushanhu Road, 230031, Hefei, Anhui, China
[2] Dipartimento di Economia, Ingegneria, Società e Impresa (DEIM), Università degli Studi della Tuscia, Campus Riello—blocco F, Largo dell' Università, 01100 Viterbo, Italy
[3] Dipartimento di Ingegneria Elettrica e Tecnologie dell'Informazione (DIETI), Università degli Studi di Napoli Federico II, via Claudio 21, 80125 Napoli, Italy
[4] Consorzio CREATE, via Claudio 21, 80125 Napoli, Italy

E-mail: adriano.mele@unitus.it

Received 22 February 2022, revised 28 April 2022
Accepted for publication 12 May 2022
Published 1 June 2022

Abstract

This article discusses the integration of a Kalman filter in the P-EFIT equilibrium reconstruction code, with the aim of estimating the currents induced in the passive structures of a tokamak. The filter is based on a vacuum electromagnetic model of the reactor, and takes advantage of an estimate of the effect of the plasma on the magnetics, provided by the equilibrium reconstruction algorithm. On the other hand, the observer is integrated into the equilibrium reconstruction, which exploits the eddy currents estimates provided by the Kalman filter to refine the obtained solution. To analyze the interplay of the reconstruction code and the proposed observer, the ITER tokamak is considered as a case-study, and the algorithm is tested on a variety of plasma conditions, selected in such a way to maximize the relevance of an accurate knowledge of the passive currents. The code performance is evaluated in terms of convergence metrics, eddy currents estimation accuracy and reconstruction of plasma-related quantities such as plasma–wall gaps, plasma current and plasma profile parameters.

Keywords: eddy currents, equilibrium reconstruction, magnetic equilibrium, ITER, P-EFIT, CREATE-NL, Kalman filter

(Some figures may appear in colour only in the online journal)

1. Introduction

The reconstruction of the plasma magnetic configuration is one of the core issues in modern tokamak diagnostics. In a tokamak, the extremely high temperature of the plasma and its susceptibility to the presence of impurities make it prohibitive to place any sensor inside the plasma region. For this reason, dedicated algorithms are usually implemented in tokamak experiments in order to reconstruct the magnetic topology inside the vacuum chamber from the available measurements. In most cases, the plasma is assumed to evolve *quasi-statically* through equilibrium states, described by a nonlinear elliptic PDE known as the Grad–Shafranov equation. This equation can be written in cylindrical coordinates (r, z, φ) as

$$\Delta^* \psi = -\mu_0 r J_\varphi (r, z, \psi), \tag{1}$$

* Author to whom any correspondence should be addressed.
[a] These authors contributed equally.

where ψ is the magnetic flux, expressed in Wb rad^{-1}, across a disk whose boundary passes through the point (r, z) of the poloidal plane, μ_0 is the vacuum magnetic permeability, J_φ is the toroidal current density, which in general depends both on the coordinates (r, z) and on the solution to the problem ψ, and Δ^* is an elliptic differential operator given by

$$\Delta^* = r\frac{\partial}{\partial r}\left(\frac{1}{r}\frac{\partial}{\partial r}\right) + \frac{\partial^2}{\partial z^2}.$$

Solving this inverse equilibrium problem is fundamental, not only for post-discharge analysis of tokamak experiments, but also for real-time control. In particular, plasma magnetic control [1], and especially *shape* control, heavily relies on the reconstruction of either plasma–wall gaps (*gap control*) or flux values at a set of given control location (*isoflux control*); in either case, the controlled quantities can be obtained once the poloidal flux map inside the vacuum chamber, or at least the plasma boundary, is known.

Over the years, many different methods have been proposed to tackle the issue of magnetic equilibrium reconstruction or plasma boundary identification. Possible methods for the identification of the plasma boundary include filamentary methods [2], harmonic expansions [3], or the Cauchy condition surface code originally developed for JT-60 and now proposed also for its upgrade JT-60SA [4]. Several different codes have also been developed with the aim of computing a full poloidal flux map estimate, such as LIUQE [5], CLISTE [6], or the widely used EFIT code [7, 8], along with its real-time implementations RT-EFIT [9] and P-EFIT [10, 11]; neural network [12] or data-driven [13] methods have also been put forward as alternative options. Moreover, even if the reconstruction method considered in this article is based on magnetic measurements only, which are usually obtained by dedicated probes mounted on the chamber walls (either internally or externally), it is worth to remark that recent advances in plasma equilibrium reconstruction involve the use of internal profile measurements (such as motional Stark effect, polarimetry or kinetic profile measurements) in order to more accurately fit the plasma internal profiles [14–18]. Moreover, in future reactors inductive-based magnetic diagnostics may not be viable. For this reason, alternative magnetic probes such as Hall sensors [19] are under study for DEMO.

However, equilibrium reconstruction algorithms may encounter difficulties in achieving a satisfactory degree of accuracy during some critical phases of a tokamak discharge, as it happens during ramp-up or ramp-down phases or during transitions between different confinement regimes, such as the LH or HL ones. One of the reasons behind this loss of accuracy is that, during these transient phases, significant passive currents are induced in the conductive structures surrounding the plasma, which are usually not measurable by means of the standard tokamak diagnostic equipment. In this view, the availability of an estimate of said currents could prove beneficial to the equilibrium reconstruction performance. Different approaches to this problem can be found in the technical literature; for example, in [20] the authors link the available measurements to an approximate representation of the plasma current density, which is then used to integrate numerically the vessel currents dynamics, while H-infinity observers have been proposed in [21, 22]. In [23], the passive elements are represented by rectangular axisymmetric circuit, and the actual expression of the field generated by a distributed current flowing in the rectangular cross section of the elements is used in the reconstruction to increase the accuracy close to the current carrying elements. Moreover, the code adopts some devices studied to take into account 3D effects, which are particularly important due to the fact that the shell quadrants of the considered experiment (LTX) are toroidally discontinuous. In this same respect, in [24] such 3D effects are considered in the reconstruction by using as a source the toroidal average of the induced passive currents computed through a 3D model of the non-axisymmetric passive structures. Finally, an attempt at the introduction of a Kalman filter based observer can be found in [25], where a plasma linearized response model is used to estimate both the induced passive currents and the shape modifications with respect to a reference equilibrium.

1.1. Contribution of this work

In the present article, a possible method to directly integrate a Kalman filter into the P-EFIT code is proposed, with the aim of improving its performance during the most delicate phases of a tokamak discharge. The observer is designed on a vacuum model of the reactor, and takes advantage of the equilibrium reconstruction code to estimate the effect of the presence of the plasma on the dynamics of the induced passive currents. On the other hand, the resulting eddy current estimates are exploited by the reconstruction algorithm to improve the equilibrium reconstruction accuracy.

P-EFIT is a parallelized version of the equilibrium reconstruction code EFIT. It is based on the CUDA™ (compute unified device architecture) framework, and runs on graphical processing unit cores to significantly accelerate the computation with respect to the original EFIT code. P-EFIT is designed to run in real-time during tokamak operations, and provides several plasma quantities which are relevant for control applications. The standard version of the code has already been integrated into the EAST plasma control system, and is routinely used in experiments for real-time plasma configuration control [10, 11].

For the purpose of this work, an off-line analysis has been carried out with P-EFIT on a set of synthetic ITER pulse segments, simulated by means of the 2D FEM code CREATE-NL [26], in order to validate the effects of the introduction of the proposed observer for the passive currents. For the proposed analysis, an equivalent axisymmetric description of the passive structures is used both for the simulation and the Kalman filter, and the results are compared to the ones obtained with the standard version of the reconstruction algorithm, in order to quantify the improvement in terms of equilibrium reconstruction accuracy.

1.2. Article overview

The rest of this document is structured as follows.

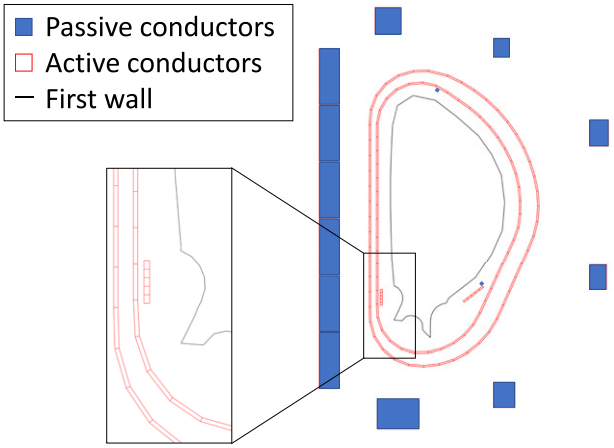

Figure 1. Poloidal cross section of the ITER tokamak 2D model used for the identification. The active coils have been highlighted in blue, while the passive structures have been discretized in 110 rectangular elements (a magnified view of the lower left region is shown as an example).

- In **section 2** the filter equations are derived and their integration in the P-EFIT code is discussed;
- **Section 3** briefly describes the synthetic measurements extracted from the simulated plasma scenario segments, the assumptions on the measurement noise and some details on how these measurements are processed by the reconstruction code;
- In **section 4** the results obtained using different configurations of the P-EFIT code equipped with the eddy currents observer on four different synthetic scenario segments are presented;
- **Section 5** concludes the article.

2. Integration of an eddy current estimator in the P-EFIT code

In this section, the equations of the Kalman filter used to estimate the currents induced in the passive structures of an equivalent 2D axisymmetric model of the machine are introduced and discussed. The filter is based on a plasmaless electromagnetic model of the reactor, obtained by means of the CREATE-L code [27], while the plasma contribution is taken into account on the basis of the equilibrium reconstruction provided by the P-EFIT code.

2.1. Assumptions

It is assumed that the machine can be described by a fully axially symmetric model. It is also assumed that the passive structures can be represented up to a satisfactory degree of accuracy by means of a set of discrete, axisymmetric circuits, as shown in figure 1. In particular, in the considered example the ITER passive structures, including the two shells of the vacuum vessel, the triangular support and the divertor rail, have been modeled as a set of 110 discrete circuits.

2.2. Tokamak electromagnetic model

To design the eddy currents observer, we consider the following electromagnetic model[5]

$$L_e\dot{I}_e + M_{ae}\dot{I}_a + \dot{\psi}_{ep} + R_eI_e = 0 \tag{2}$$

where the symbols have the following meaning:

- I_e vector of the currents in the passive circuits (to be estimated)
- I_a vector of the active currents flowing in the CS & PF circuits (measured)
- ψ_{ep} vector of the flux produced by the plasma on the passive circuits (evaluated by P-EFIT)
- L_e passive structures inductance matrix
- M_{ae} mutual inductance matrix between active and passive circuits
- R_e passive structures (diagonal) resistance matrix

The (vacuum) inductance and resistance matrices L_e, M_{ae}, R_e are evaluated offline by means of the CREATE-L code, while the plasma contribution ψ_{ep} is to be computed by the P-EFIT code.

Then, in order to avoid the time differentiation of I_a and ψ_{ep}, the following state transformation is introduced

$$\psi_e = L_eI_e + M_{ae}I_a + \psi_{ep} \tag{3}$$

where ψ_e is the flux linked with the passive circuits. From this equation, it immediately follows that

$$\dot{\psi}_e = -R_eI_e = -R_eL_e^{-1}\psi_e + R_eL_e^{-1}M_{ae}I_a + R_eL_e^{-1}\psi_{ep} \tag{4}$$

which can be put in standard state-space form

$$\dot{\psi}_e = A\psi_e + BI_a + E\psi_{ep} \tag{5}$$

defining

- $A = R_eL_e^{-1}$
- $B = R_eL_e^{-1}M_{ae}$
- $E = R_eL_e^{-1}$

Notice that I_a and ψ_{ep} are considered as external inputs to the system.

2.3. Measurements

The measurements (obtained from sensors such as magnetic field probes, full flux loops, saddle loops) can be described by means of the following equation:

$$m = C_eI_e + C_aI_a + m_p \tag{6}$$

where m is the measurements vector, C_e and C_a are vacuum matrices (again computed by the CREATE-L code) and m_p is the plasma contribution to the measurements, that must be evaluated by P-EFIT. From (3) we obtain, in terms of the transformed state variables ψ_e

$$m = C\psi_e + DI_a + F_1\psi_{ep} + F_2m_p \tag{7}$$

[5] The considered model is a modified version of the typical plasma response linearized model produced by the CREATE-L code; for details, see [27].

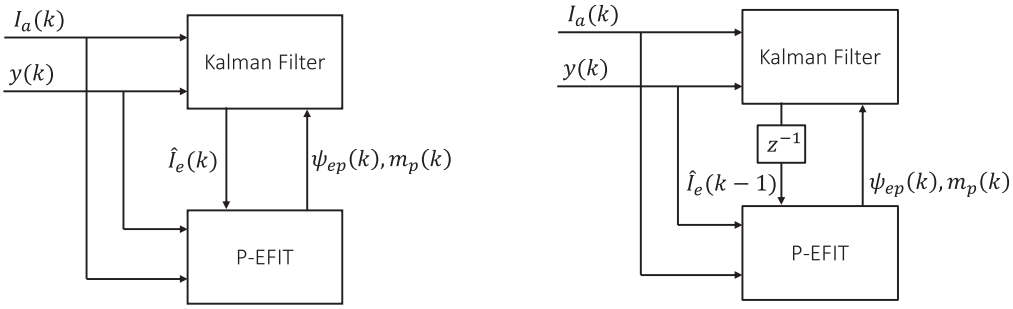

(a) Integration scheme between the standard P-EFIT code and the Kalman filter.

(b) A time delay is introduced to break the algebraic loop in the coupling mechanism.

Figure 2. Integration of the Kalman filter in the P-EFIT code.

where

- $C = C_e L_e^{-1}$
- $D = C_a - C_e L_e^{-1} M_{ae}$
- $F_1 = -C_e L_e^{-1}$
- F_2 is the identity matrix

Observe that, if the plasma is represented by a set of filamentary currents, as it is done in P-EFIT, then

$$\psi_{ep} = G_1 \mathcal{I}_p, \qquad m_p = G_2 \mathcal{I}_p \tag{8}$$

where the G_1 and G_2 matrices elements are the Green functions that link said filaments to the considered measurements, while $\mathcal{I}_p$ is the vector of filamentary currents that represents the plasma[6]. The positions of these filaments correspond to the nodes of the code computational grid, which means that the G_1 and G_2 matrices can be pre-computed offline. At each iteration, only the filaments that fall inside the (estimated) plasma region are allowed to carry a non-zero current. As it often happens in equilibrium reconstruction codes, in P-EFIT the distribution of these currents is constrained by expressing the plasma internal current density profile through a polynomial expansion, whose coefficients are estimated as part of the fitting procedure [11].

2.4. Time discretization

From equations (3), (5) and (7), the following discrete-time model can be obtained:

$$\begin{aligned} \psi_e(k+1) &= \tilde{A}\psi_e(k) + \tilde{B} I_a(k) + \tilde{E}\psi_{ep}(k) \\ I_e(k) &= \tilde{M}_e \psi_e(k) + \tilde{M}_a I_a(k) + \tilde{M}_p \psi_{ep}(k) \\ m(k) &= \tilde{C}\psi_e(k) + \tilde{D} I_a(k) + \tilde{F}_1 \psi_{ep}(k) + \tilde{F}_2 m_p(k) \end{aligned} \tag{9}$$

where the expression of the matrices denoted with the ˜ superscript depends on the discretization method chosen. In the implementation discussed in this work, the discretization has been obtained simply by using Matlab's `c2d` command with the `'zoh'` option, choosing a sample time of 1 ms.[7]

[6] The symbol $\mathcal{I}_p$ is used to avoid confusion with the total plasma current I_p.

[7] The typical execution time of P-EFIT for each reconstruction iteration on the considered hardware architecture is in the order of 600–700 μs.

2.5. Interaction of the Kalman filter with the P-EFIT code

The Kalman filter is used to provide the estimated value of the passive currents $\hat{I}_e(k)$ to P-EFIT, while in turn the P-EFIT code must provide the Kalman filter with an estimation of the $\psi_{ep}(k)$ and $m_p(k)$ terms. A simple integration scheme is shown in figure 2(*a*).

Unfortunately, it can be immediately noticed that this simple scheme contains an algebraic loop, as P-EFIT needs the estimation of the passive currents at time k in order to compute the plasma contribution at the same instant, while the Kalman filter needs the plasma contribution at the same time instant k in order to provide $\hat{I}_e(k)$ to the reconstruction algorithm. To break this loop, a time delay can be introduced in the scheme of figure 2(*a*), obtaining the scheme shown below in figure 2(*b*).

It is worth to observe that, with this method of integration, the P-EFIT code simply considers the passive circuits as additional current measurements. In the Grad–Shafranov equation solver of P-EFIT, the contribution of the passive currents on the magnetic measurements and on the poloidal flux values at the nodes of the grid is given by

$$\begin{aligned} m &= G_p^m \mathcal{I}_p + G_a^m I_a + G_e^m I_e \\ \psi_{grid} &= G_p^{grid} \mathcal{I}_p + G_a^{grid} I_a + G_e^{grid} I_e \end{aligned} \tag{10}$$

where G_p^m, G_a^m and G_e^m are the Green-table functions that link the magnetic measurements to the current sources, while G_p^{grid}, G_a^{grid} and G_e^{grid} are the Green-table functions between the poloidal magnetic flux on the grid nodes and the current sources. It is worth to notice that *ad-hoc* post-processing functions are needed in order to evaluate the ψ_{ep} and m_p terms.

2.6. Kalman filter equations

For the proposed application, a steady-state Kalman filter has been used. The Kalman steady-state gain matrix is hence defined as:

$$L^\infty = A P^\infty \tilde{C}^T (C P^\infty \tilde{C}^T + N)^{-1} \tag{11}$$

where the filter gain matrix L^∞ depends on the chosen state and measurements covariance matrices. In particular, N is the

Algorithm 1. P-EFIT with eddy currents estimator.

Require: pre-compute the G_{p}^{m}, G_{a}^{m}, G_{e}^{m}, $G_{\mathrm{p}}^{\mathrm{grid}}$, $G_{\mathrm{a}}^{\mathrm{grid}}$ and $G_{\mathrm{e}}^{\mathrm{grid}}$ Green matrices; choose initial guess for the eddy currents $\hat{I}_{\mathrm{e}}(0)$ (e.g. zero initial condition) and the initial poloidal flux map $\psi(0)$ (e.g. simple circular plasma); choose maximum number of iterations per time step (`maxiter`) and convergence tolerance (`eps`)
solve the Grad–Shafranov problem at first iteration until convergence based on $I_{\mathrm{a}}(0)$, $m(0)$, $\hat{I}_{\mathrm{e}}(0)$
for $k = 0$, $k \leqslant n$. of samples, $k{+}{+}$ **do**
▷ Kalman filter step
compute $\psi_{\mathrm{ep}}(k)$ and $m_{\mathrm{p}}(k)$
compute the residuum $r(k)$ based on (13b)
obtain a prediction for $\psi_{\mathrm{e}}(k+1)$ through (13c)
obtain a new estimate for the eddy currents from (13a)
▷ Standard P-EFIT algorithm
`niter` $= 0$
`psierr` $= \infty$
while `niter` $\leqslant$ `maxiter` AND NOT `psierr` $<$ `eps` **do**
solve (1) at time step k based on $I_{\mathrm{a}}(k)$, $m(k)$, $\hat{I}_{\mathrm{e}}(k)$
compute convergence error `psierr` as in (2)
`niter` $+{+}$
end while
end for

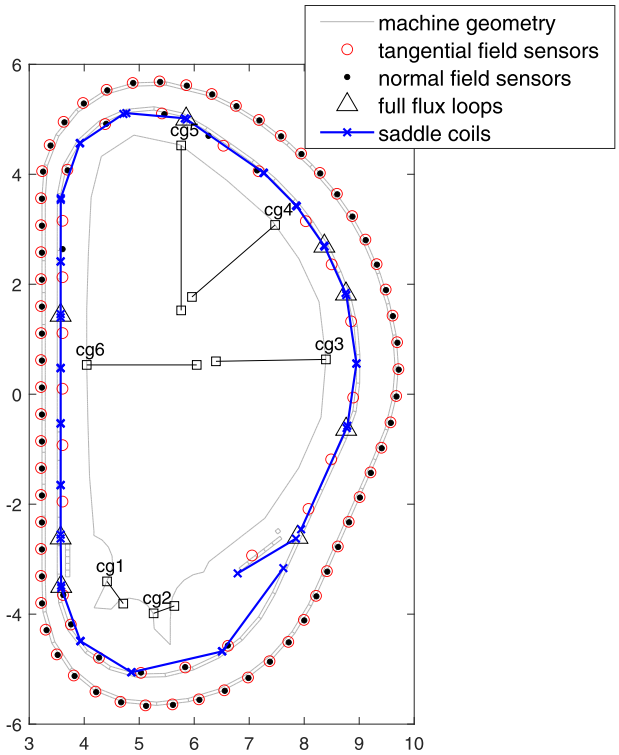

Figure 3. Available magnetic sensors and choice of gaps for the accuracy assessment.

measurement covariance matrix, while P^{∞} is the solution of the algebraic Riccati equation

$$P^{\infty} = \tilde{A}P^{\infty}\tilde{A}^{\mathrm{T}} - AP^{\infty}\tilde{C}^{\mathrm{T}}(\tilde{C}P^{\infty}\tilde{C}^{\mathrm{T}} + N)^{-1}\tilde{C}P^{\infty}\tilde{A}^{\mathrm{T}} + \tilde{B}W\tilde{B}^{\mathrm{T}} \tag{12}$$

Table 1. Measurements error expressed in terms of 2σ. Note that, for the saddle coils, the absolute error is expressed in mT, as it is normalized to the coil area. The 2σ value of the drift term $n_{2,v}$ is assigned assuming a discharge of 3600 s.

Sensor category	$n_{1,f}$ (%)	$n_{1,s}$	$n_{2,c}$	$n_{2,v}$
55.AA	0.20	0.22%	1.5 mT	8.4 mT
55.AB	0.20	0.22%	1.5 mT	8.4 mT
55.AD	0.01	≈0	≈0	1.8 mT
55.AE	0.20	0.17%	—	9.7 mWb
55.AF	0.20	0.03%	—	5.4 mWb
55.A3	0.02	0.20%	1.5 mT	5.4 mWb
55.A4	0.02	0.20%	1.5 mT	0.2 mT
55.A7	0.02	0.17%	—	0.6 mWb

in which the covariance matrix of the active current measurement noise is denoted by W.

The resulting Kalman filter equations are:

$$\hat{I}_{\mathrm{e}}(k) = \tilde{M}_{\mathrm{e}}\psi_{\mathrm{e}}(k) + \tilde{M}_{\mathrm{a}}I_{\mathrm{a}}(k) + \tilde{M}_{\mathrm{p}}\psi_{\mathrm{ep}}(k) \tag{13a}$$

$$r(k) = m(k) - \left[\tilde{C}\psi_{\mathrm{e}}(k) + \tilde{D}I_{\mathrm{a}}(k) + \tilde{F}_1\psi_{\mathrm{ep}}(k) + \tilde{F}_2 m_{\mathrm{p}}(k)\right] \tag{13b}$$

$$\psi_{\mathrm{e}}(k+1) = \tilde{A}\psi_{\mathrm{e}}(k) + \tilde{B}I_{\mathrm{a}}(k) + \tilde{E}\psi_{\mathrm{ep}}(k) + L^{\infty}r(k). \tag{13c}$$

In particular, (13a) represents the relation between the magnetic fluxes linked to the considered circuits and the estimated passive currents, (13b) is the expression of the fitting residuum and (13c) represents the Kalman filter prediction/correction step. The quantities $\psi_{\mathrm{ep}}(k)$ and $m_{\mathrm{p}}(k)$ are provided by the equilibrium reconstruction code at time (k) on the basis of the active currents $I_{\mathrm{a}}(k)$, of the actual plasma measurements at time step (k) and of the estimated eddy currents (see figure 2(b)).

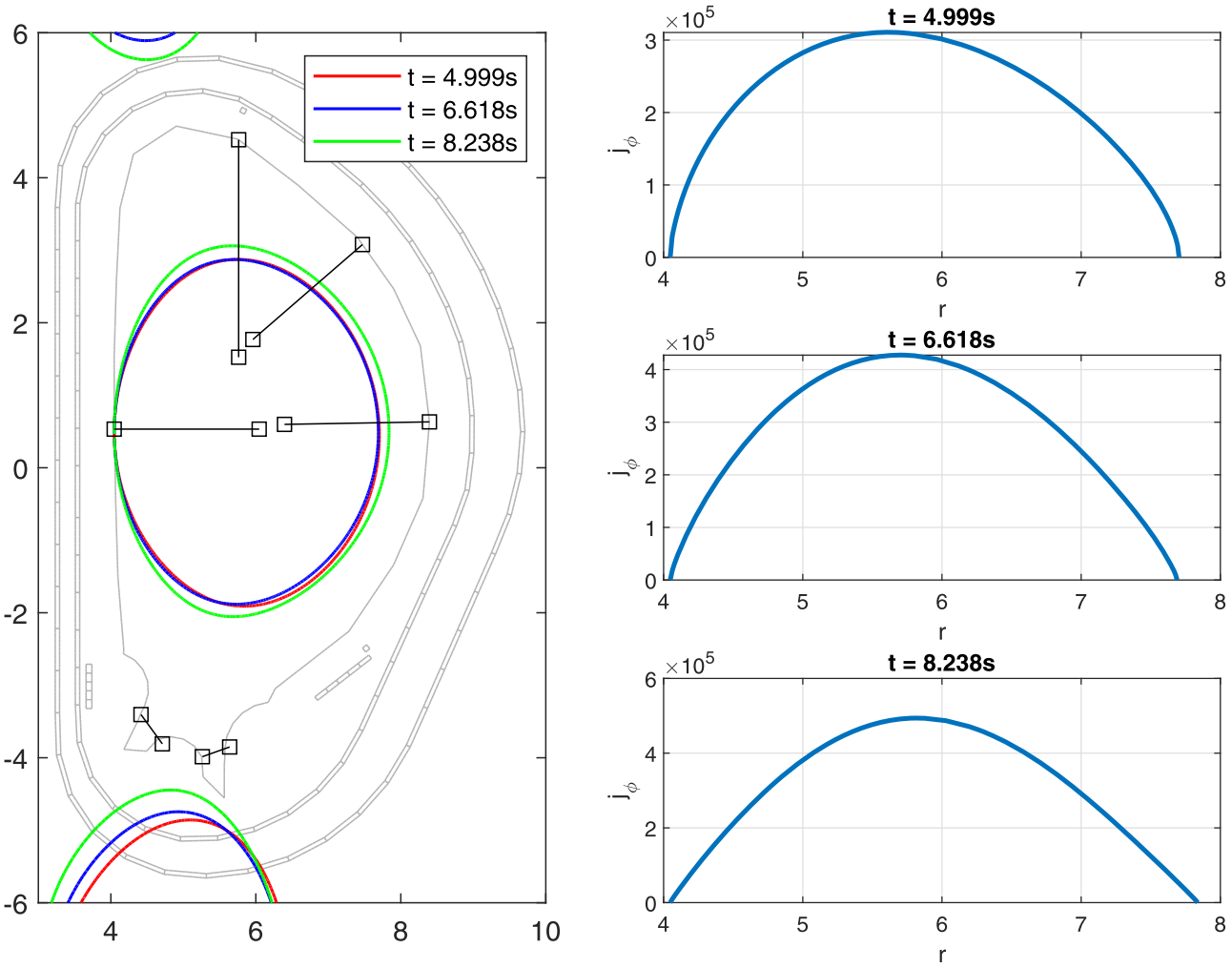

Figure 4. On the left, the plasma boundary at the initial, middle and final time instants of the considered segment. On the right, the internal plasma current density profiles associated to the same snapshots (taken along a horizontal line passing through the plasma centroid).

Finally, it is worth to recall [11] that, for each plasma snapshot, the convergence criterion for P-EFIT is defined on the basis of the difference between the poloidal flux map obtained in two successive iterations. In particular, a plasma equilibrium reconstruction is considered to have reached convergence if the following condition is satisfied in all of the grid nodes

$$\frac{|\psi^{(k+1)} - \psi^{(k)}|}{|\psi_a - \psi_b|} < \varepsilon \tag{14}$$

where $\psi^{(k)}$ is the flux at iteration k in the considered node, ψ_a is the flux at the magnetic axis, ψ_b is the flux at the boundary and ε is a tolerance parameter. However, for real-time operation, the number of iteration is usually fixed (to 1 or 2 per time step), and this quantity is often regarded as a metric to assess the quality of the obtained reconstruction rather than as a termination criterion. Another useful figure of merit to evaluate the quality of the reconstructed plasma configuration is the so-called χ^2, i.e. the quantity which is minimized by the fitting procedure, which is defined as

$$\chi^2 = \sum_{i=1}^{n_M} \frac{m_i - \tilde{m}_i}{\sigma_i} \tag{15}$$

where m_i and $\tilde{m}_i$ are the calculated and measured output of the ith probe respectively, σ_i is the associated uncertainty, and n_M is the total number of measurements.

The coupled equilibrium reconstruction/eddy current estimation algorithm is schematically described in algorithm 1.

3. Synthetic plasma pulse data

In order to assess the performance of the proposed algorithm both in term of equilibrium reconstruction improvement and accuracy in the eddy currents estimation, a set of different plasma scenario segments have been taken into account. In particular, the following situations have been considered:

(a) First phase of the ramp-up with very low I_p
(b) Ramp-up phase following (a)
(c) End of plasma current ramp-up & SOF with LH transition
(d) End of flat-top & HL transition

These segments were chosen because they were expected to be the ones where the benefit in estimating the eddy currents and including them in the equilibrium reconstruction is

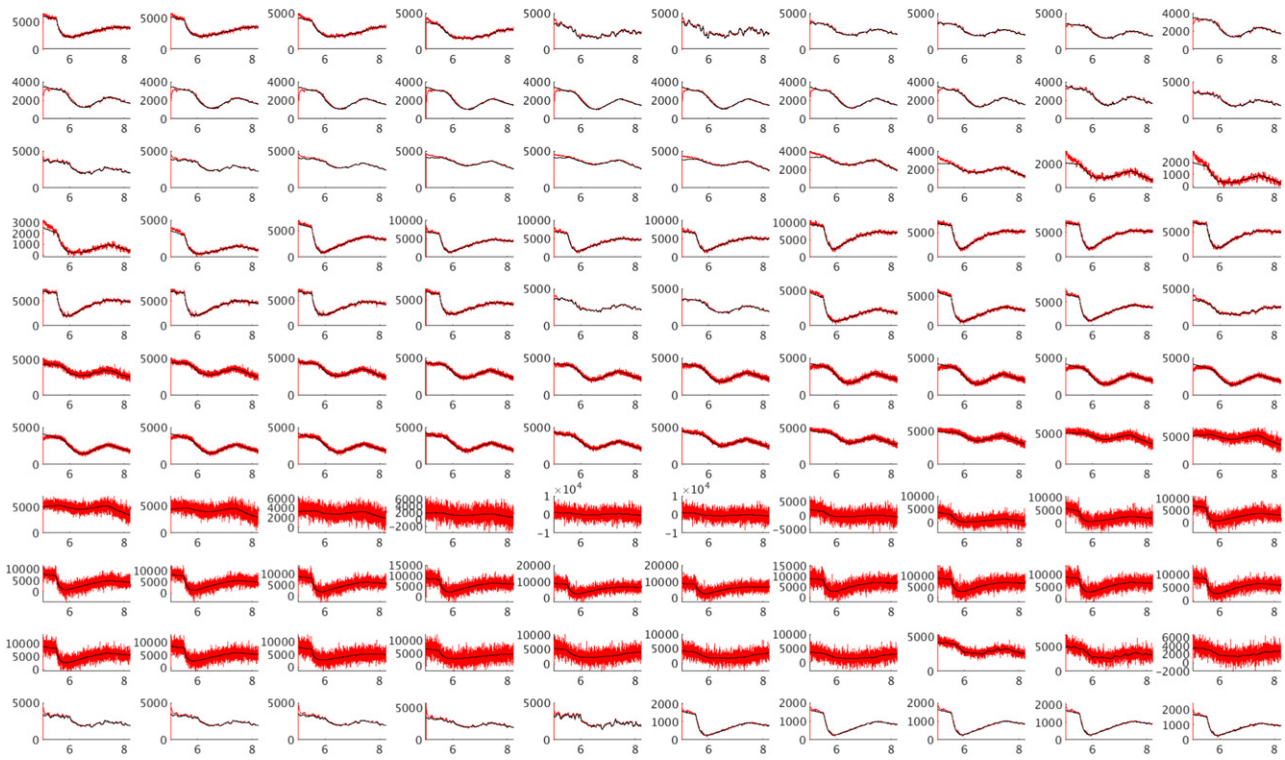

Figure 5. Comparison between eddy currents simulated by CREATE-NL (black) and the estimated ones (red) on each passive structure. No low pass filtering is applied to the PF coils currents measurements. The first five rows (elements from 1 to 50) show the currents in the conductors of the inner shell, rows six–ten (elements 51–100) contain the passive currents on the outer shell, while the last row (elements 101–110) shows the passive currents on the passive plates.

maximum. In particular, the Kalman filter has been tuned on segment (b), which was used to choose the filter covariance matrices and to analyze the effect of different choices of sensors and of the application of a low-pass filtering action with different cutoff frequencies to the active currents measurements (see sections 3.1 and 4.1).

More details about each of these segments are given in section 4. The different considered plasma scenarios have been simulated by means of the nonlinear evolutionary code CREATE-NL [26], a 2D FEM code that solves the free-boundary plasma equilibrium problem and couples it to the dynamic behavior of the currents flowing in the active coils, in the passive structures and in the plasma itself. CREATE-NL has been used and validated on a variety of different devices over the years, such as JET [28, 29], TCV [30], EAST [31–33] and JT60-SA [34–36].

3.1. Measurements

From the simulated scenario data, several different synthetic magnetic measurements have been extracted. In particular, the following set of ITER measurements has been considered for the equilibrium reconstruction[8]:

- AA inner tangential field sensors (24 sensors)
- AB inner normal field sensors (12 sensors)
- AD inner partial flux loops (22 sensors)
- AE inner continuous flux loops (eight sensors)
- AF compensated diamagnetic flux
- Active CS & PF coils currents
- Estimate of the plasma current (obtained as a linear combination of the in-vessel magnetic measurements)

while for the Kalman filter the following ones have been taken into account:

- Inner vessel sensors:
  - AA inner tangential field sensors (24 sensors)
  - AB inner normal field sensors (12 sensors)
  - AD inner partial flux loops (22 sensors)
  - AE inner continuous flux loops (eight sensors)
- Outer vessel sensors
  - A3 outer tangential field sensors (60 sensors)
  - A4 outer normal field sensors (60 sensors)
  - A7 outer continuous flux loop (six sensors)
- Active CS & PF coil currents

In addition to that, the case where the Kalman filter only uses the inner vessel sensor measurements (combined with the active coil currents measurements) has been considered in the tuning phase, as discussed in section 4.1. The position of the inner and outer vessel sensors used for the assessment is shown in figure 3, together with the selection of plasma–wall gaps used to verify the shape reconstruction accuracy of the code.

[8] The labels make reference to the standard ITER sensors nomenclature.

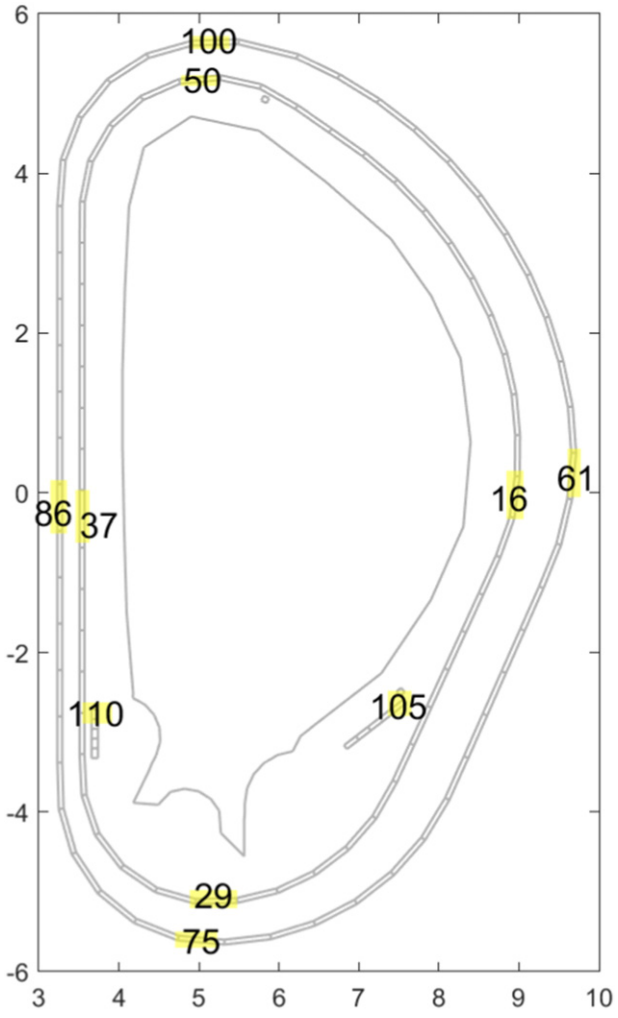

Figure 6. Selection of passive structures for results visualization.

For more details on the ITER diagnostics system, the reader is referred to [37].

3.2. Measurement noise

The synthetic measurements have been corrupted with a simulated measurement noise. To this aim, it has been assumed that each sensor measurement can be written as

$$y = y_0(1 + n_{1,f} + n_{1,s}) + n_{2,c} + n_{2,v} \tag{16}$$

with

- $n_{1,f}$ relative measurement error contribution which changes rapidly over time (e.g. due to electronics)
- $n_{1,s}$ relative measurement error contribution which changes slowly over time (e.g. calibration and thermal errors)
- $n_{2,c}$ absolute measurement error contribution whose statics do not change over a pulse (e.g. cross-talk)
- $n_{2,v}$ absolute measurement error contribution whose statics do change over a pulse (e.g. integrator drifts due to electronic offsets and irradiation effects)

Each measurement error component has been separately characterized from a statistical point of view, specifying its distribution and the related parameters (e.g. mean and variance). The details of this analysis are beyond the scope of this article; an overview of the results is given table 1.

Moreover, it was also assumed that the measured and actual currents are linked through the following relation

$$I_{\text{meas}} = I_0(1 + n_r) + n_a$$

with $2\sigma_{n_r} = 0.002$ (i.e. 0.2%), $2\sigma_{n_a} = 7A$.

An important aspect to be taken into account for the plasma equilibrium reconstruction is the impact of the spatial modes $n < 3$. To compensate the effect of these modes, the input measurements can be obtained by averaging signals coming from corresponding sensors placed in different machine sectors equally spaced at a toroidal distance of 120°. When this procedure is taken into account, the error on each measurement is reduced by a factor $1/\sqrt{3}$ with respect to the single sensor statistics. Moreover, this procedure allows to compensate for 3D modes that have a toroidal harmonic number that is not a multiple of 3.

As a final note, it is worth to observe that the active CS & PF coils currents enter the estimation of the eddy currents throughout equations (13a) and (13b); in particular, looking at equation (13b) it can be noticed that the CS & PF coils measurement noise directly affects the estimated values of the eddy currents without any filtering action. This is true, in particular, for the passive elements which belong to the outer shell, which are closer to the active circuits and are more heavily affected by the noise on the measurements of their currents. On the other hand, the effect of the noise on the elements in the internal structures is partially filtered by the outer shell itself. This can be seen clearly in figure 5, where the noisiest estimates are those associated to the eddy current in the outer shell elements.

To overcome this drawback, the active currents in input to the Kalman filter, at the choice of the user, can be filtered by a discrete first order low-pass filter (LPF) with equation:

$$Y(n) = a * X(n) + (1 - a) * Y(n - 1) \tag{17}$$

where $a = 2\pi f_c T_s$, f_c being the cut-off frequency of the filter, and T_s the sample time, $X(n)$ is the unfiltered input at the nth time step, and $Y(n)$ is the filter output. In order to take into account this filtering action directly in the Kalman filter design phase, (a) a dynamic model for the active CS & PF circuital currents and (b) the use of the measurements of the voltages applied to these circuits would be required. Since these measurements are not yet well defined for the ITER tokamak, in the present paper the LPF (17) has not been considered in the observer design.

4. Simulation results

In this section, the results obtained running the P-EFIT code equipped with the Kalman filter eddy current estimator on the synthetic plasma scenario segments listed in section 3 are discussed, and the performance of the code is assessed in terms

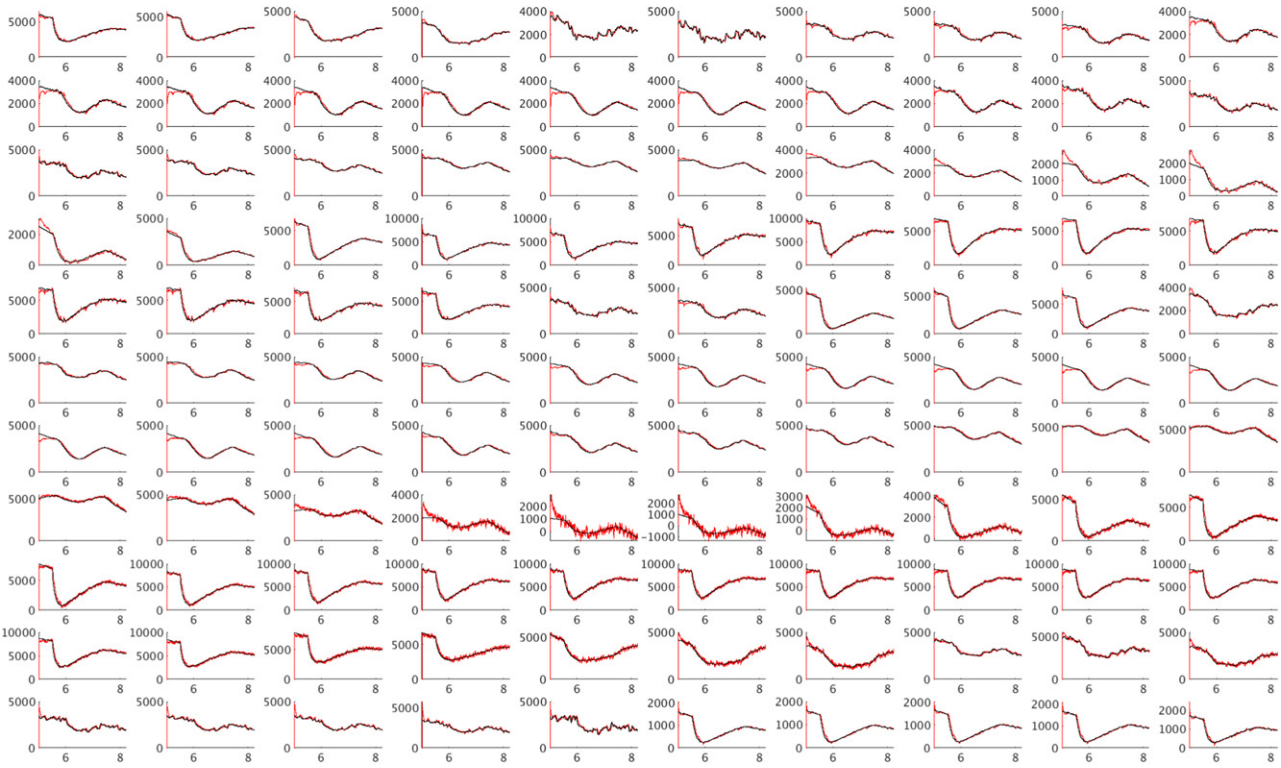

Figure 7. Comparison between eddy currents simulated by CREATE-NL (black) and the estimated ones (red on each passive structure. A LPF with a cut-off frequency of 5 Hz is applied to the PF coils currents measurements. The introduction of the filter significantly reduces the noise on the estimated eddy currents, while leaving the plasma shape almost unaffected, as shown in figure 8.

of accuracy of the reconstruction of some plasma parameters. The main code parameters used for the runs are listed below:

- The size of the grid used by P-EFIT for the analysis is 129×129;
- If not explicitly stated, the equilibrium reconstruction, at each time step, is carried out by P-EFIT by performing a single iteration of the optimization procedure used to fit the measurements, as in the real-time case. The filter performance when using a larger number of iterations is discussed at the end of section 4.1 (see figure 13);
- For the analysis of a single segment, the initial plasma equilibrium for the streaming procedure is calculated by waiting for the reconstruction of the first snapshot to converge. Since this initial reconstruction typically takes about 20–30 iterations, in the practical case the streaming procedure would approximately start with a 20–30 ms delay. This procedure, in the case of real pulses, can be applied by P-EFIT only once, at the beginning of the pulse;
- The initial values of the eddy current in each segment were assumed to be known. Note that this is not a critical assumption, since the Kalman filter can start to estimate the eddy currents at a time instant where they are small (for instance, just before the breakdown phase), and in any case the filter typically takes 2–3 s to reach steady state, after which the effect of the initial conditions is negligible (since the response to the initial conditions decays exponentially). Anyway, this time span is negligible when compared to the length of a typical ITER pulse, which is expected to be in the order of 1 h. It is worth to remark that this initial time must be allowed for the filter to converge to an unbiased estimate of the plant state, as the initial value of the eddy currents is unknown (unless the filter is switched on in a phase of the discharge where the currents can be assumed to be negligible). This however does not mean that the estimator is not capable of tracking variations in the induced passive currents which are characterized by a faster time scale, as it can be seen, for instance, in figure 11 at time $\sim$6 s or in figure 30 at time $\sim$530 s.

In this performance assessment, only the in-vessel sensors have been used for the equilibrium reconstruction, while the Kalman filter takes into account both in and out-vessel sensors measurements. Moreover, measurements of the CS & PF currents are used in both cases. Each sensor measurement has been corrupted by an additive noise signal according to what is described in section 3.1.

4.1. Plasma ramp-up

The first scenario segment, described in this section, is actually the continuation of the initial ramp-up segment described in section 4.2; however, since this segment was used to tune the Kalman filter, it is the first to be discussed.

For this pulse segment, the plasma is in an elongated limiter configuration, with a plasma current ramping from 2.48 MA up to 3.36 MA. The total value of the eddy currents on the passive

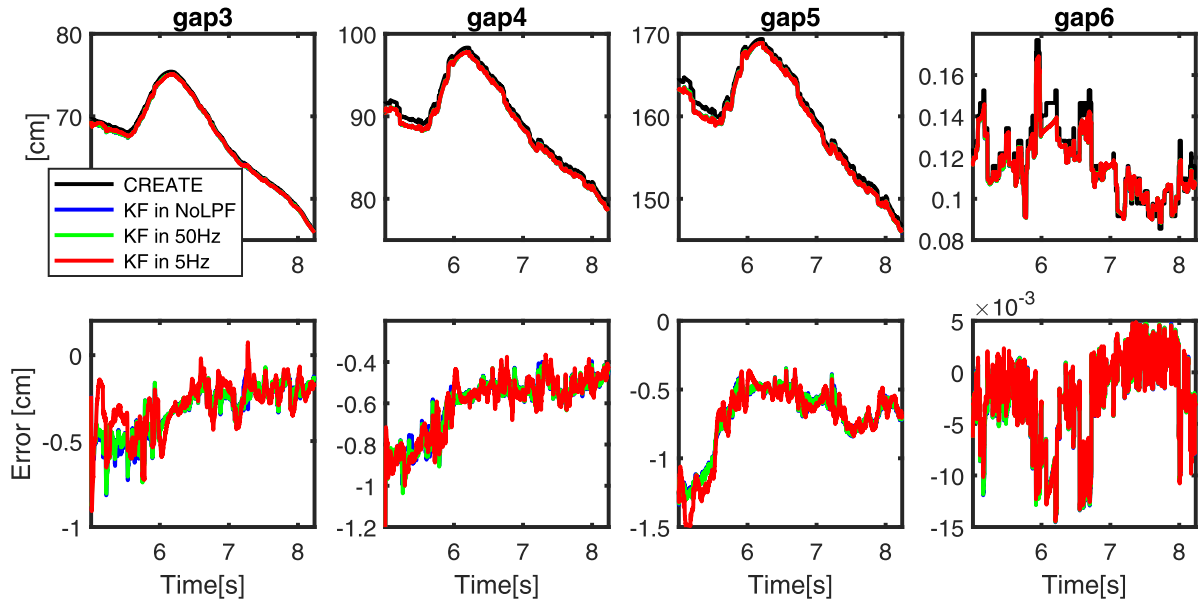

Figure 8. Gap reconstruction results for P-EFIT with Kalman filter using only in-vessel sensors (gaps #1 and #2 are not plotted for limiter configurations). The results with no LPF on the PF coil currents measurements are shown in blue, the ones where a 50 Hz cut-off frequency has been chosen are shown in green, while the results with a cut-off of 5 Hz are shown in red. The results obtained with different tunings of the LPF almost overlap, showing that the filter has no particular effect on the plasma shape reconstruction.

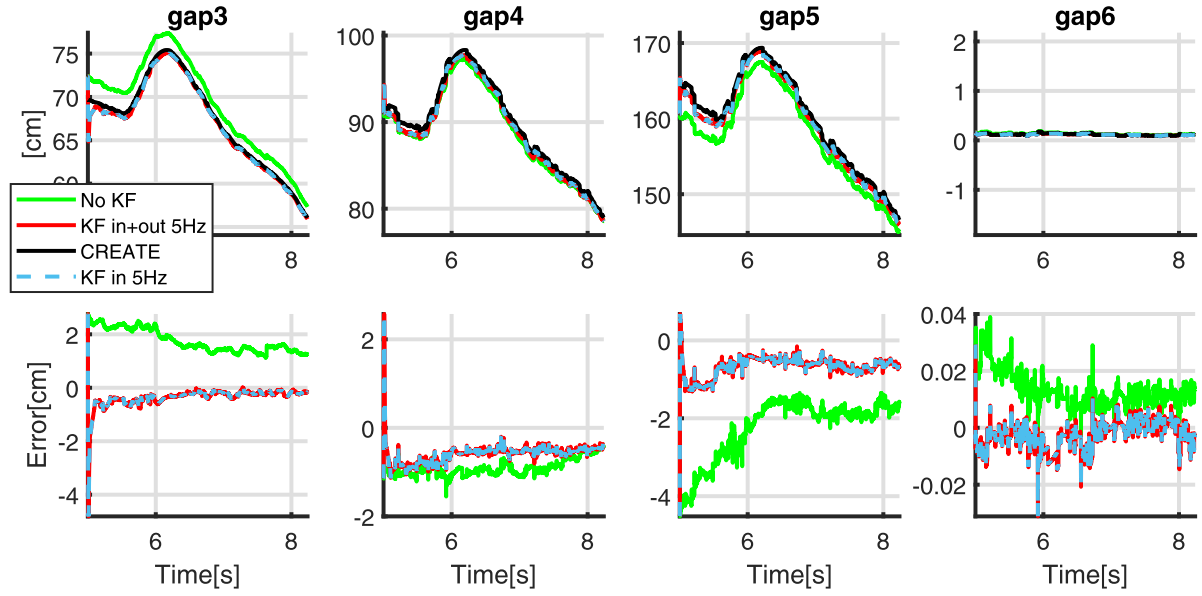

Figure 9. P-EFIT gap results (gaps #1 and #2 are not considered for limiter configurations). The results obtained with the Kalman filter using only in-vessel sensors are shown by the dashed blue trace, while the results with Kalman filter using both in-vessel and out-vessel sensors are shown in red. The green traces show the results when P-EFIT run without using the Kalman filter, while the simulated quantities to be estimated are shown in black.

structures goes from 519 kA to 302 kA, which is a significant fraction of the total plasma current (of about the 20% at the beginning of the segment). Plasma boundary snapshots taken at the beginning, middle and end of the segment, together with the associated internal current density profiles, are shown in figure 4.

In figure 5, the reconstruction results obtained for all the 110 considered passive currents are shown. It can be seen how the current reconstruction is very noisy on some of the considered passive elements, particularly those that are part of the outer shell (the inner shell contains elements from 1 to 50, the outer shell elements 51–100, while elements 101–110 are located in the passive plates; see also figure 6).

As discussed in section 3.1, in order to reduce the noise on the estimated eddy currents, the measured active currents fed to the Kalman filter were smoothed by means of a LPF. In particular, to choose the cutoff frequency of the filter, its effect on both the estimated eddy currents and the reconstructed plasma shape has been considered. In particular, from figure 7 it can be seen that a cutoff frequency of 5 Hz (i.e. 10π rad s^{-1}) is

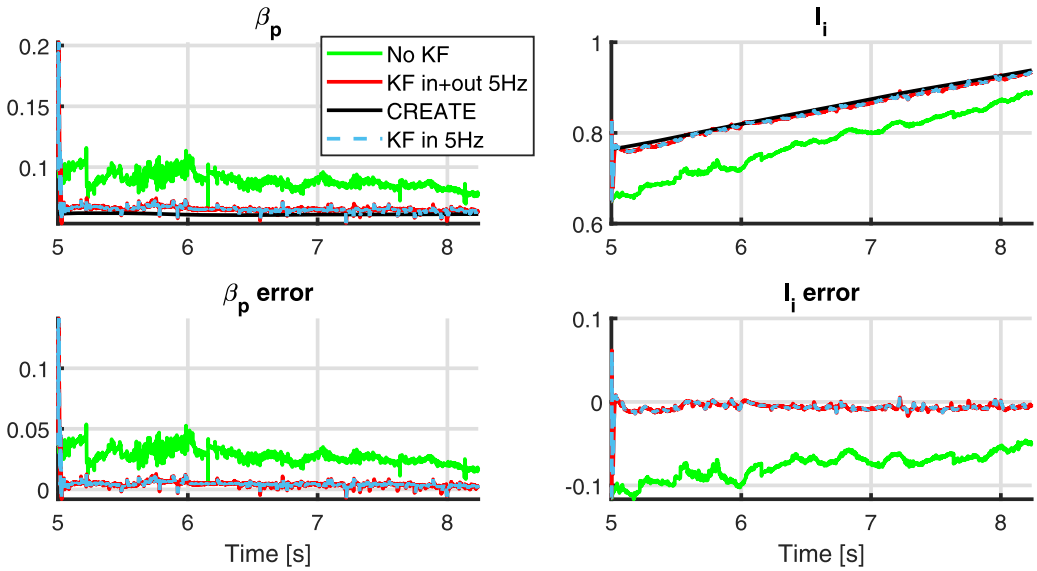

Figure 10. P-EFIT results in terms of the reconstruction of the β_p and l_i parameters. The results obtained with the Kalman filter using only in-vessel sensors are shown by the dashed blue trace, while the results with Kalman filter using both in-vessel and out-vessel sensors are shown in red. The green traces show the results when P-EFIT is run without using the Kalman filter, while the simulated quantities to be estimated are shown in black.

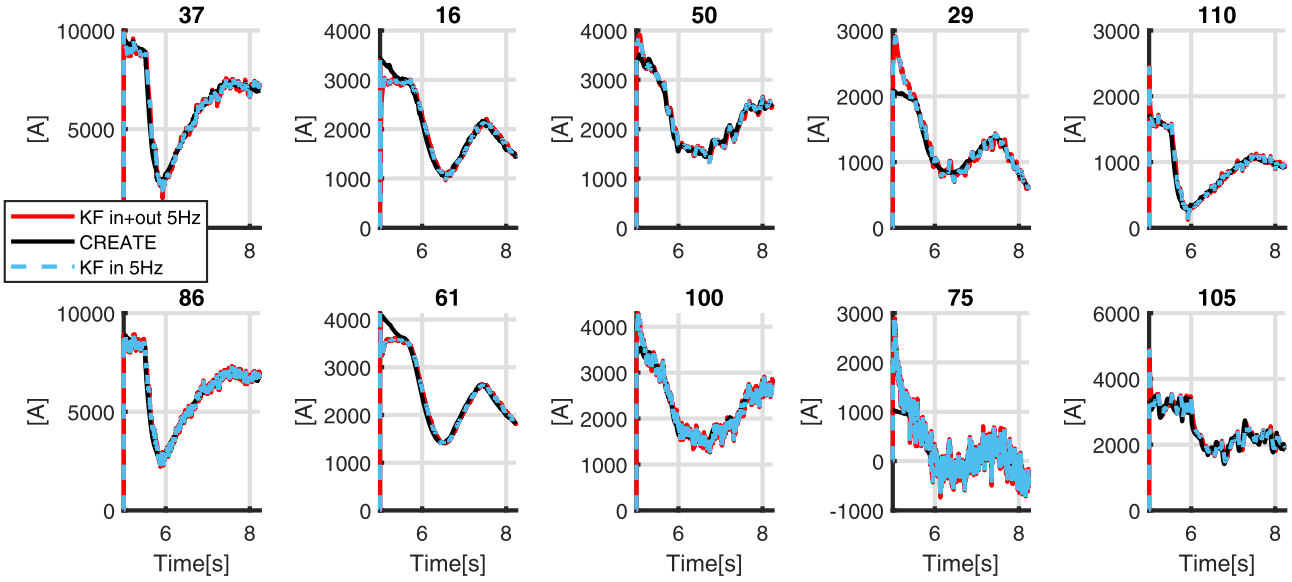

Figure 11. Eddy currents estimated on the elements of figure 6 with a LPF on the active currents measurements with a cut-off frequency of 5 Hz.

already enough to significantly reduce the noise on the estimated passive currents, while the results in figure 8 indicate that the effect of the filtering action on the estimated gaps is negligible. This observation is consistent with the fact that the outer shell structure is located farther from the plasma and, as a consequence, the currents flowing that structure have a smaller impact on the plasma shape.

Another significant aspect to be considered is the choice of the measurements to be used by both the reconstruction algorithm and the Kalman filter. The present version of P-EFIT allows the user to choose two separate sets of sensors, one for the reconstruction algorithm and the other for the passive currents observer. As discussed in section 3.1, for the present analysis we chose to feed the GS solver with the in-

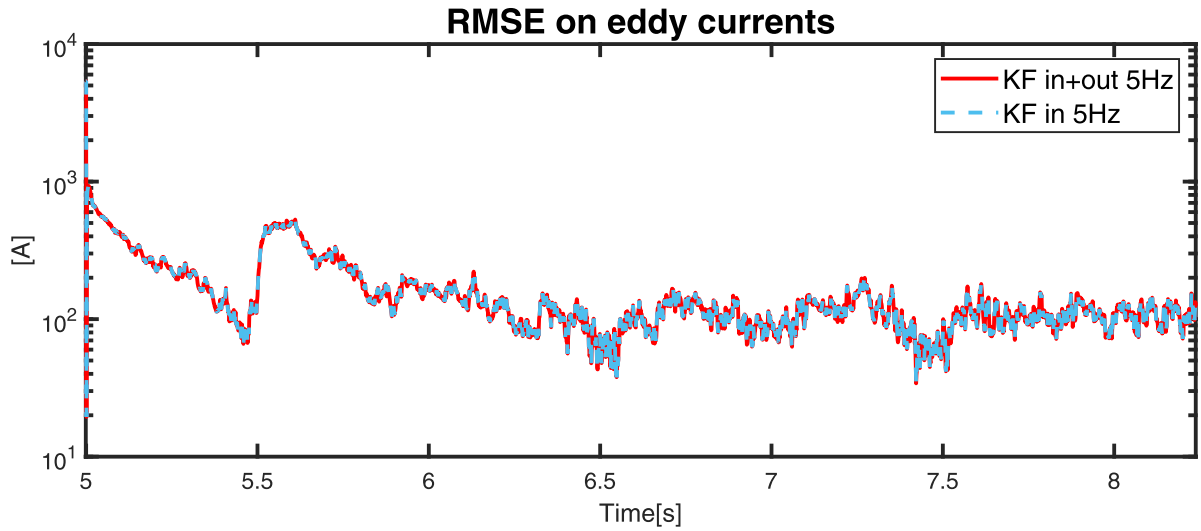

Figure 12. Root-mean-square error on all the reconstructed passive in the case where only in-vessel sensors are used (blue dashed) and where both in-vessel and out-vessel measurements are considered (red). A LPF on the active currents measurements with a cut-off frequency of 5 Hz has been applied.

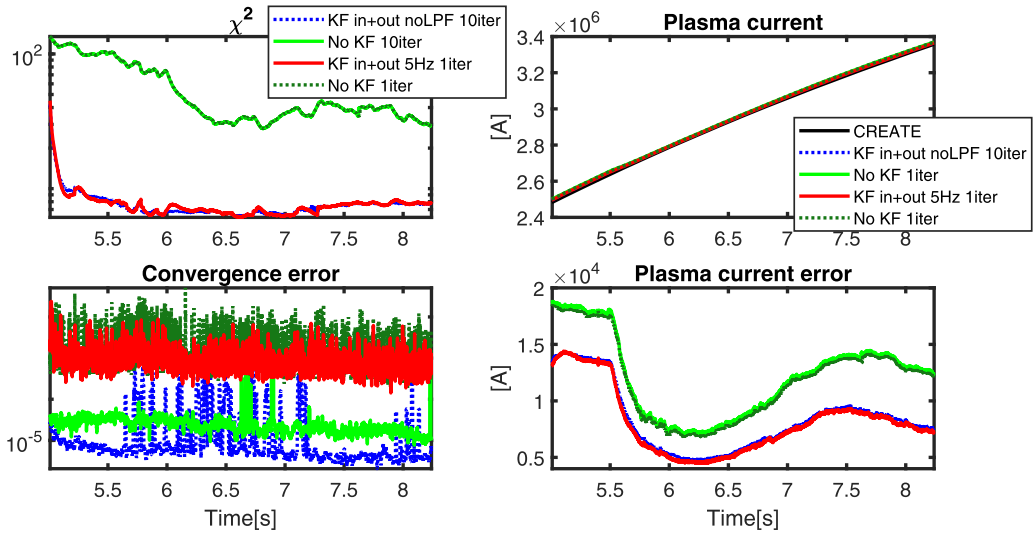

Figure 13. χ^2, convergence error, plasma current and plasma current estimation error for different settings of the P-EFIT code (refer to the main text for details).

vessel measurements only, while the Kalman filter exploits both in-vessel and out-vessel measurements. However, in order to verify the effects of this choice, some tests were carried out feeding the Kalman filter with both considered sets of sensors. Figures 9–11 show the performance of the P-EFIT code with the Kalman filter eddy current estimator in the case where only in-vessel measurements are considered and in the case where both in and out-vessel sensors are used; in particular, the accuracy in the reconstruction of the plasma–wall gaps, of the β_p and l_i plasma parameters and of a selection of eddy currents, chosen so as to represent different regions of the passive structures, as shown in figure 6, is considered. The RMSE on all the passive currents is also shown in figure 12. As it can be seen, the results are basically identical in the two considered cases. For this analysis, the code has been run with a 5 Hz LPF with one iteration per time-step. It can also be seen how the introduction of the Kalman filter is beneficial to the accuracy of the equilibrium reconstruction, as the error on both the estimated gaps and plasma parameters is significantly reduced.

Finally, the performance of the P-EFIT code in the different considered cases is evaluated in terms of the χ^2 metric, of the convergence error, defined in equation (2), and of the accuracy in terms of the fitting of the total plasma current I_p. From figure 13 it can be seen how, already when only one iteration per time step is performed, the results in terms of the convergence metric (2) are slightly improved by the use of the Kalman filter (solid red trace) with respect to the standard case (dotted dark green). Furthermore, when more iterations are considered (ten in the proposed example), the availability of an estimate of the eddy currents allows to achieve a significantly better accuracy, in terms of the same metric (2), with

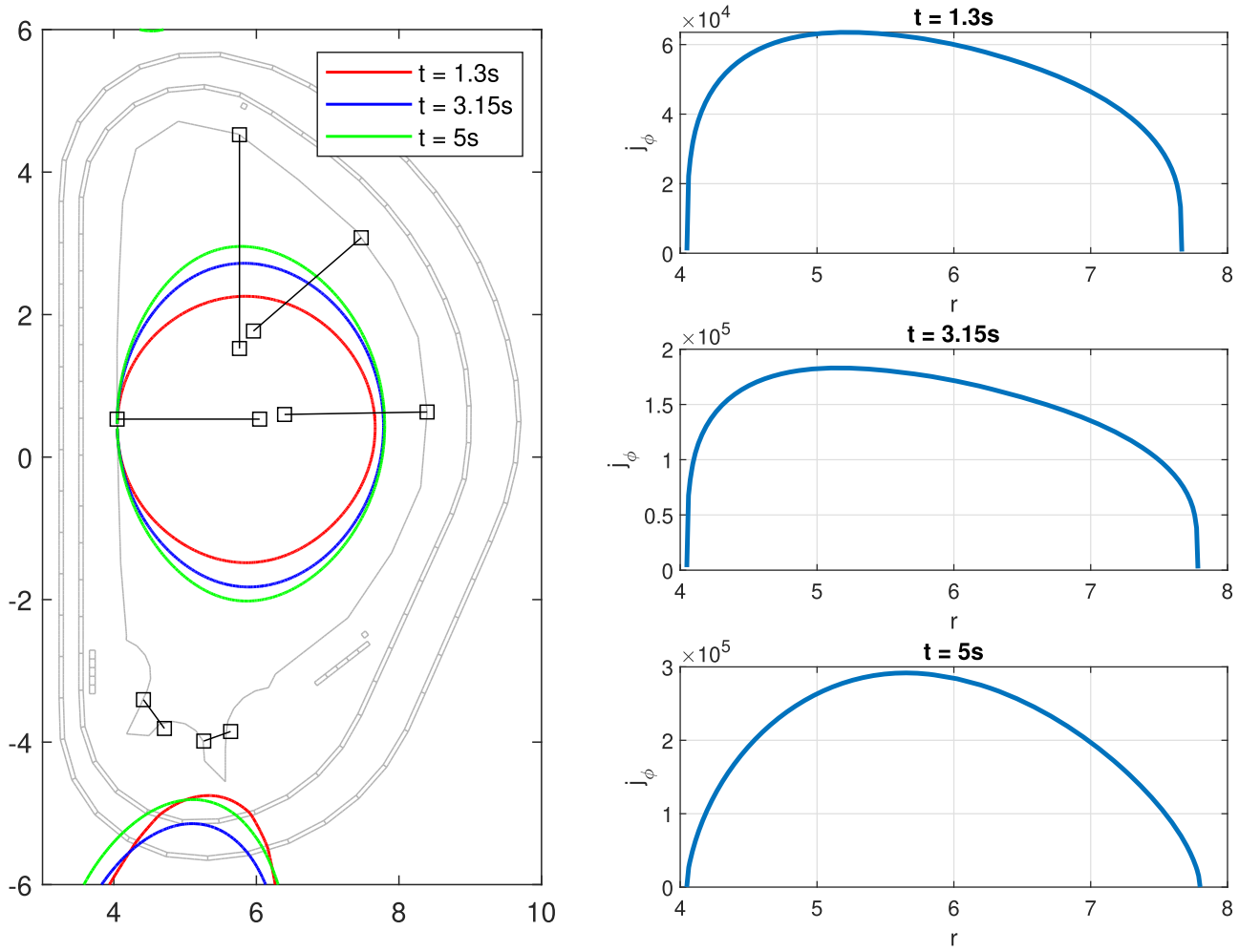

Figure 14. On the left, the plasma boundary at the initial, middle and final time instants of the considered segment. On the right, the internal plasma current density profiles associated to the same snapshots (taken along a horizontal line passing through the plasma centroid).

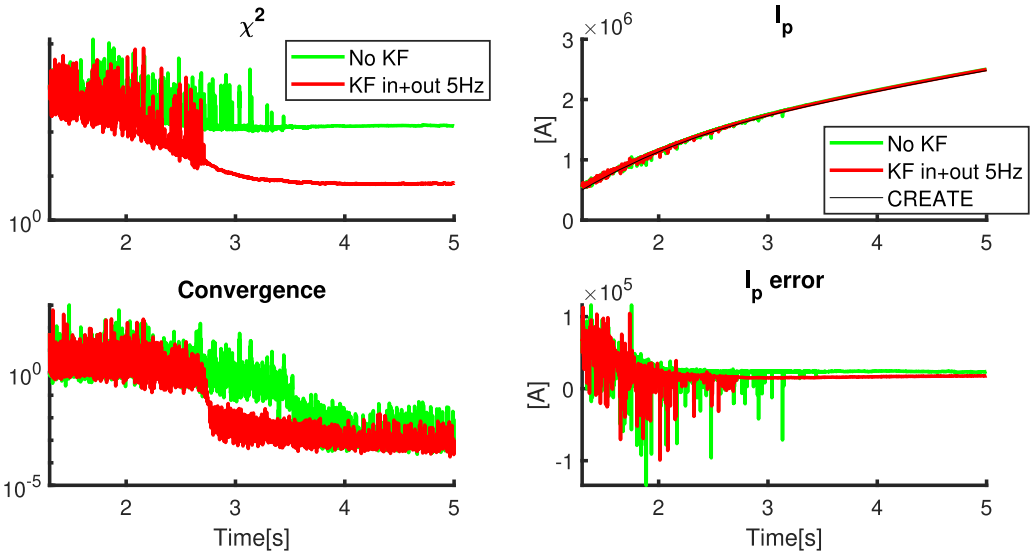

Figure 15. Magnetic reconstruction fitting χ^2, convergence and plasma current fitting (on a logarithmic scale). On the right, the plasma current fitting and fitting error.

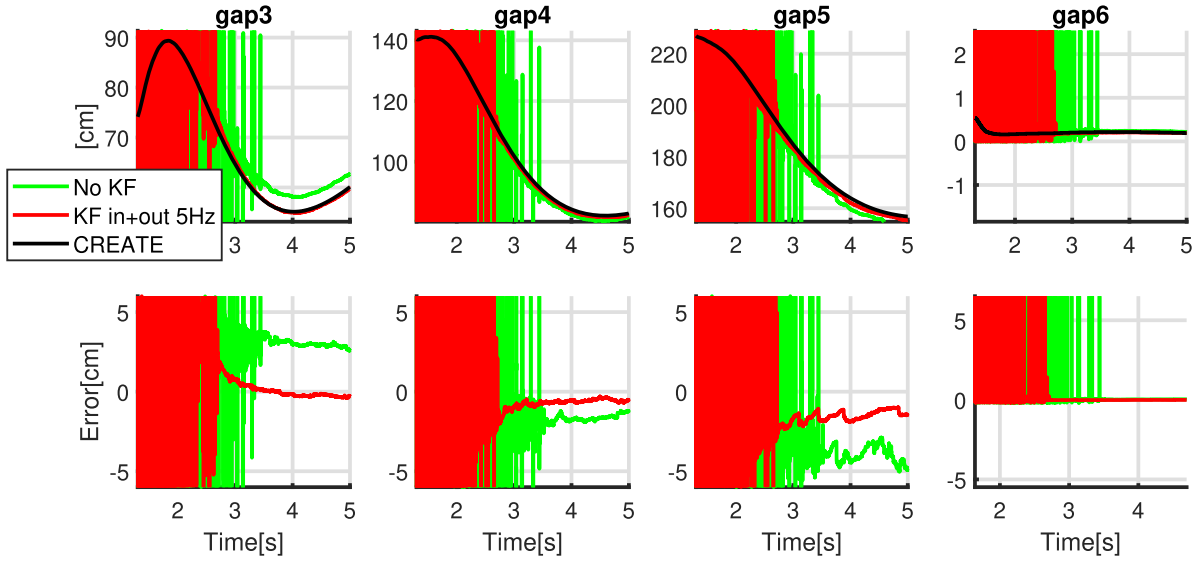

Figure 16. P-EFIT gap results (gaps #1 and #2 are not considered for limiter configurations). The black traces show the simulated gaps obtained with CREATE-L. The results obtained with the Kalman filter using in-vessel and out-vessel sensors are shown in red, while the green traces show the results without Kalman filter.

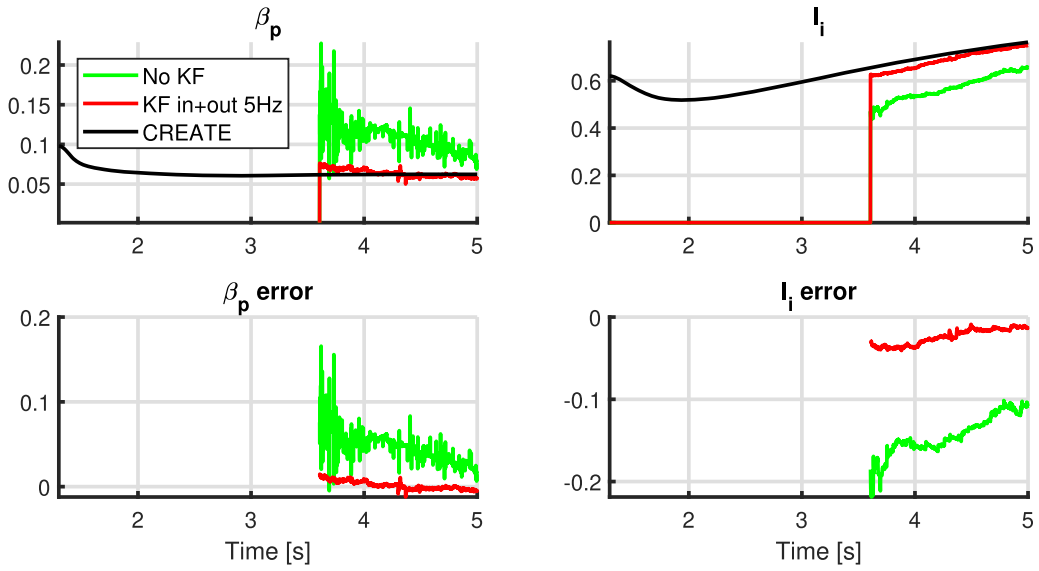

Figure 17. P-EFIT results in terms of the reconstruction of the β_p and l_i parameters. The results with Kalman filter using both in-vessel and out-vessel sensors are shown in red, while the green traces show the results when P-EFIT is run without the Kalman filter. The quantities simulated by CREATE-NL are shown in black. Notice that P-EFIT switches on the estimation of β_p and l_i when I_p reaches the value of 2 MA.

respect to the case where the same number of iterations is used, but the eddy currents are not taken into account. Moreover, it can be seen that, already in the case where only one iteration is allowed, the χ^2 value drops of about one order of magnitude with respect to the case where the Kalman filter is switched off. In this case, increasing the number of iterations does not seem to have a significant impact. The accuracy in terms of the total plasma current fitting is also improved by the presence of the filter (even though in this case the fitting error is already almost negligible in the standard case).

At this point, it is worth to make the following remark. As it was discussed, in figure 13 it can be observed how the χ^2 metric and the I_p fitting error are almost identical regardless of the number of iterations, both in the cases when the Kalman filter is used and in those where it is not switched on. The lower fitting error values are achieved by taking into account the estimate of the eddy currents, as expected. On the other hand, by using a larger number of iterations, the convergence error is reduced in both cases, and the lowest values are obtained by combining a large number of iterations with the use of the Kalman filter (blue dotted line in figure 13). In this latter case, the convergence error drops to a very low value of about 10^{-5} or less, which basically indicates that the code has reached almost full convergence (full convergence

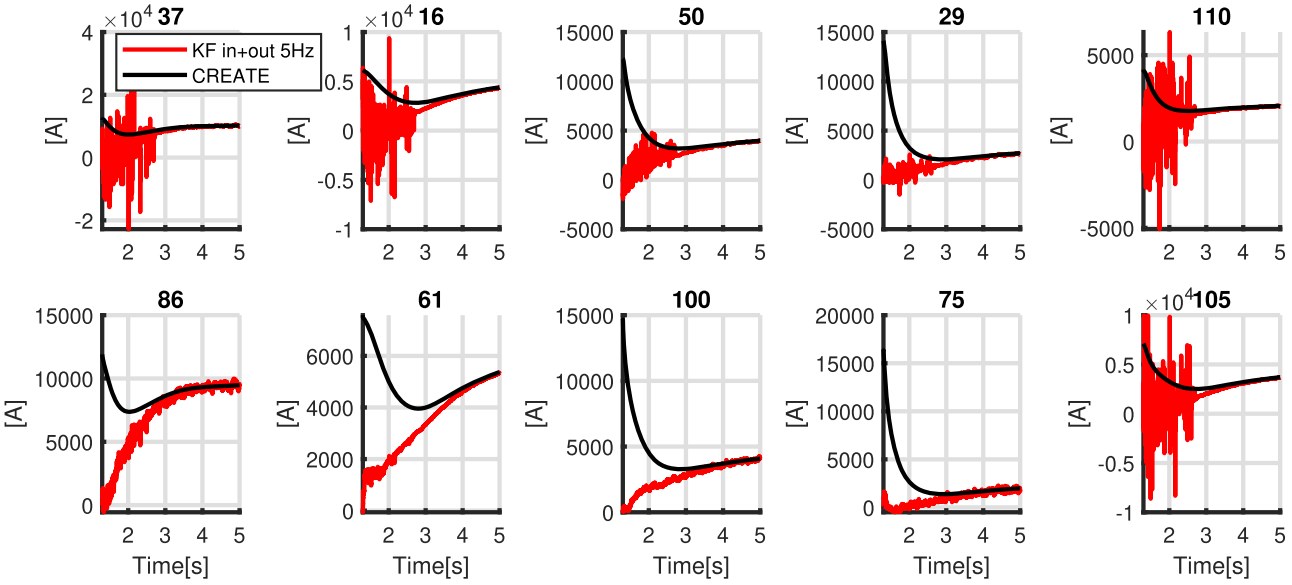

Figure 18. Comparison of eddy current on a selection of passive structures. The results obtained with the Kalman filter using in-vessel and out-vessel sensors are shown in red, while the black trace shows the simulated CREATE-L eddy currents.

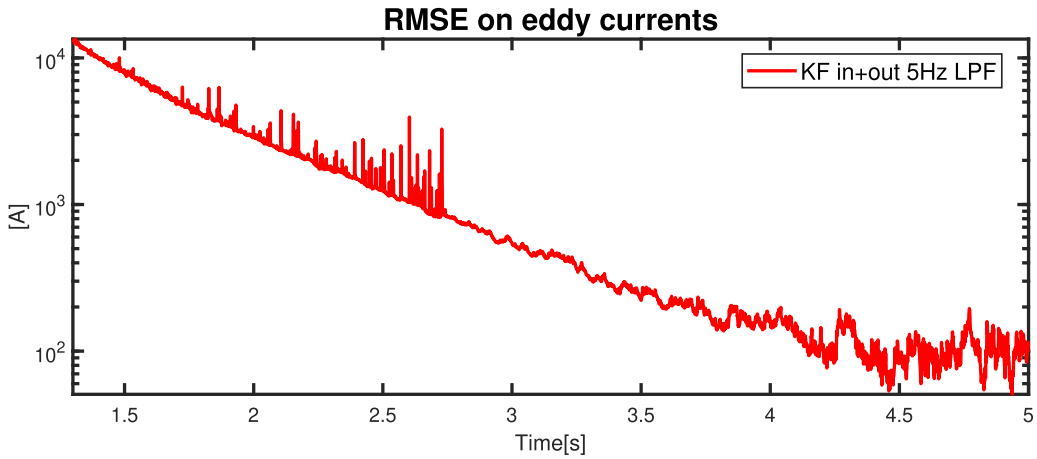

Figure 19. Root-mean-square error on the estimated currents in the 110 discretized passive conductors. The RMSE decreases from about 10^4 A to about 100 A as the Kalman filter estimates converge to the correct values.

in offline analyses is usually associated to a residual convergence error of 10^{-5}–10^{-6}; the residual noisy behavior seen in the figure can be ascribed to the lack of the LPF in the considered run). This suggests that, already with one iteration (as in the standard real-time case), the inclusion of a Kalman filter for the observation of the induced eddy currents is beneficial to the equilibrium reconstruction accuracy, as both the χ^2 metric and the I_p fitting error are significantly reduced. Moreover, a side effect of the inclusion of the Kalman filter is that the code converges faster, as a lower convergence error is achieved with the same number of iterations. This last fact is of course beneficial in offline analyses, where it indicates that full convergence is reached earlier (and hence less iterations and, subsequently, less computational time are required in total); however, it affects real-time operation as well, as consecutive reconstructions are usually very similar and hence the code is expected to achieve a good degree of convergence in less iterations also in this case.

Finally, note that, in this analysis, the case where only in-vessel sensors are fed to the Kalman filter is omitted for clarity. Anyway, the results are almost identical to the ones obtained with both in-vessel and out-vessel sensors.

From the considerations above, for the rest of the test cases presented in this work it was chosen to run the passive currents estimator using both in-vessel and out-vessel measurements and with a LPF on the active currents with a cutoff frequency of 5 Hz. In order to evaluate the performance of the code in the realistic scenario of real-time operation, only one iteration per time step has been performed.

4.2. Initial plasma ramp-up

The next analyzed segment is a limiter plasma with a very low plasma current ramping from 0.55 MA to 2.49 MA. Plasma

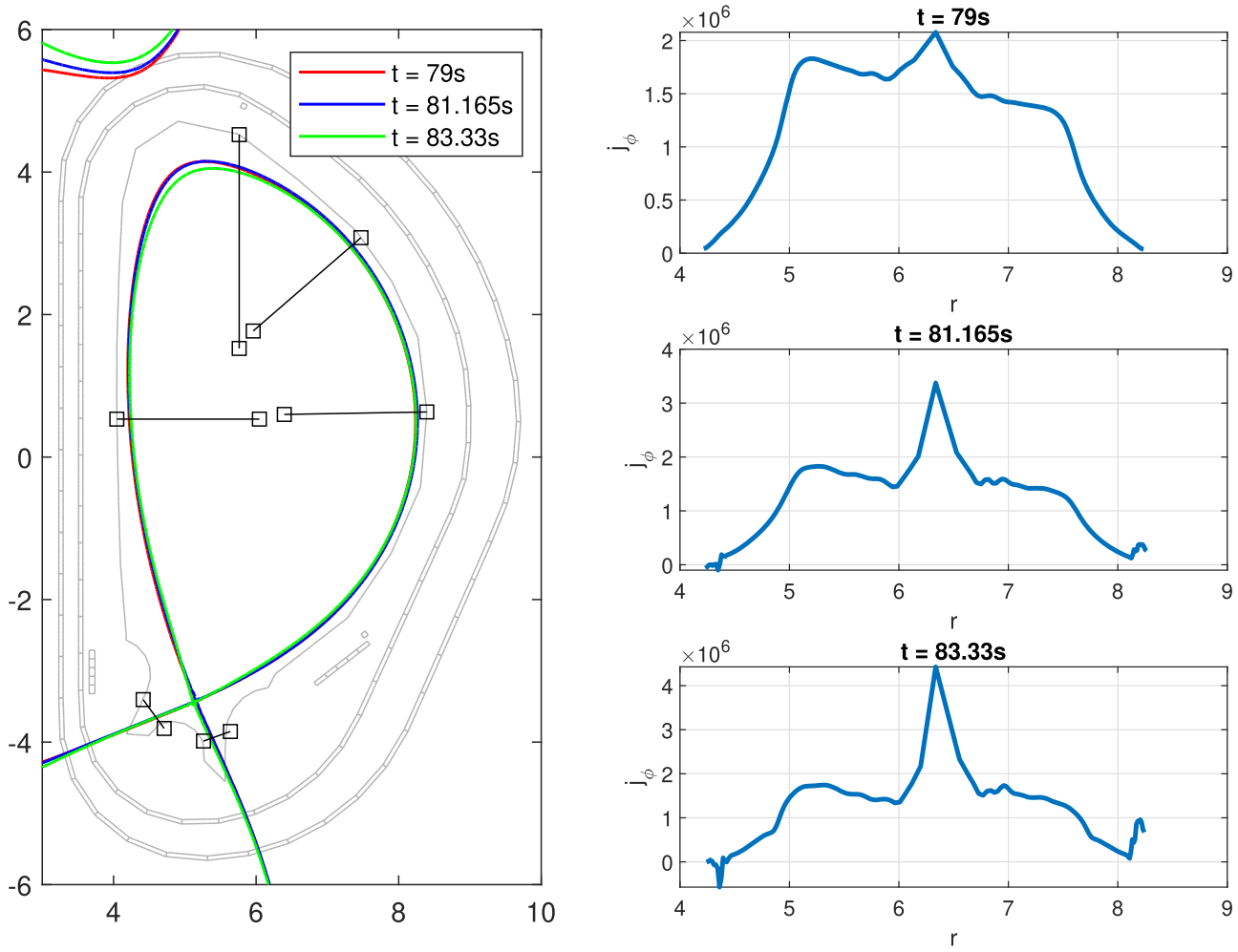

Figure 20. On the left, the plasma boundary at the initial, middle and final time instants of the considered segment. On the right, the internal plasma current density profiles associated to the same snapshots (taken along a horizontal line passing through the plasma centroid).

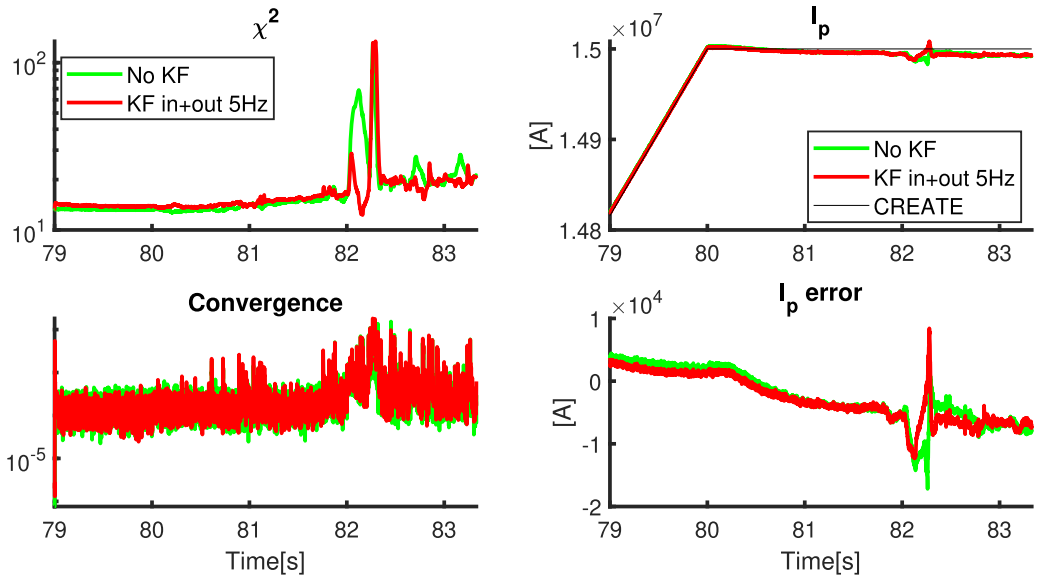

Figure 21. Magnetic reconstruction fitting χ^2, convergence and plasma current fitting (on a logarithmic scale). On the right, the plasma current fitting and fitting error.

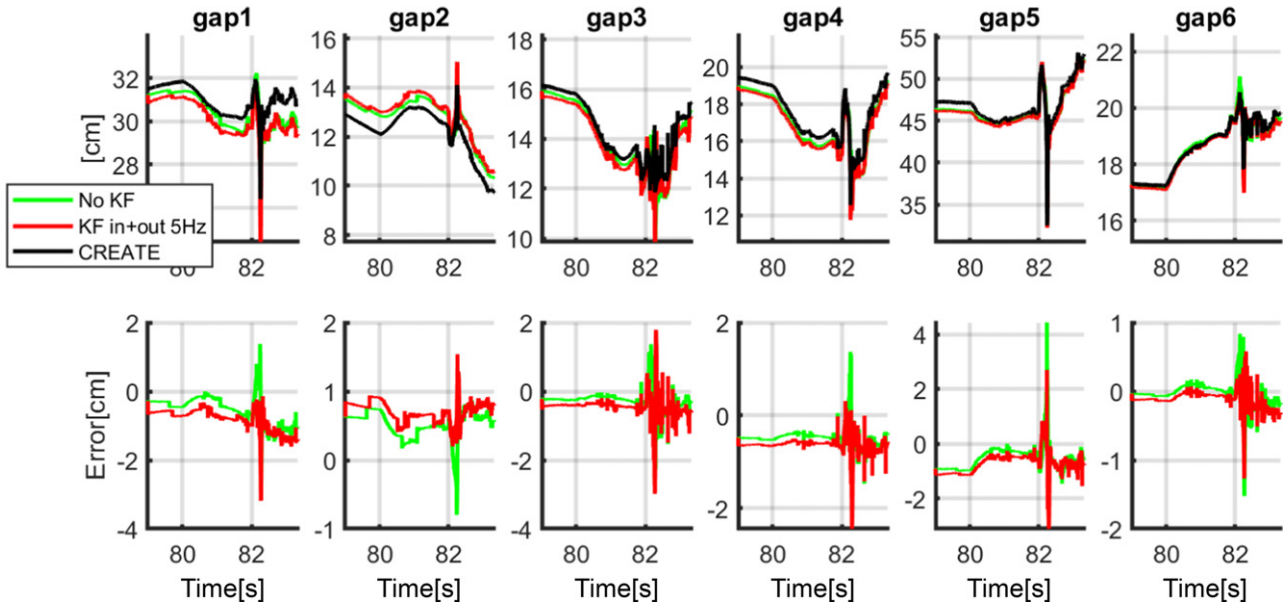

Figure 22. P-EFIT gap results (gaps #1 and #2 are not considered for limiter configurations). The black traces show the simulated gaps obtained with CREATE-L. The results obtained with the Kalman filter using in-vessel and out-vessel sensors are shown in red, while the green traces show the results without Kalman filter.

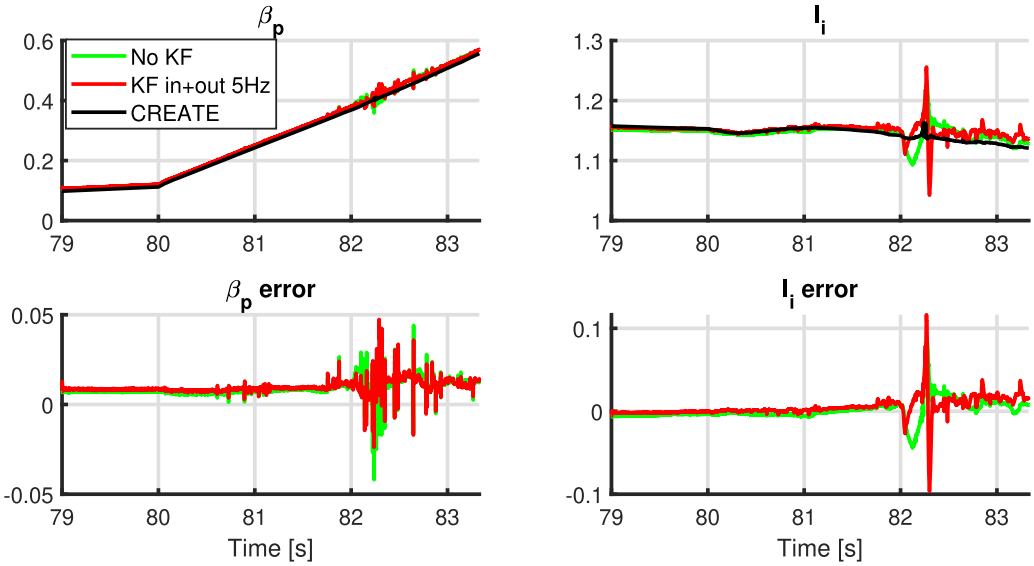

Figure 23. P-EFIT results in terms of the reconstruction of the β_p and l_i parameters. The results with Kalman filter using both in-vessel and out-vessel sensors are shown in red, while the green traces show the results when P-EFIT is run without the Kalman filter. The quantities simulated by CREATE-NL are shown in black.

boundary snapshots taken at the beginning, middle and end of the segment, together with the associated internal current density profiles are shown in figure 14.

In this case, to evaluate the transient performance of the observer, zero eddy currents have been considered in the initial state guess.

After the introduction of the Kalman filter, the χ^2 metric drops of about one order of magnitude, and both the convergence and plasma current fitting errors are also reduced, as it can be seen from figure 15. The estimated plasma–wall gaps strongly oscillate in the initial portion of the segment, as low I_p, small plasma configurations are notoriously the most critical for equilibrium reconstruction codes. However, when compared to the results obtained without the use of the Kalman filter, the eddy current estimator improves the overall equilibrium reconstruction quality, providing stable results about 0.8 s earlier than what is achieved without the estimator. In a real-world scenario, this would allow to switch on the plasma shape control earlier in the discharge, which could prove beneficial, for example, if view of an anticipated limiter to divertor transition. The gap reconstruction accuracy is also increased with respect to the standard P-EFIT version, and the estimate

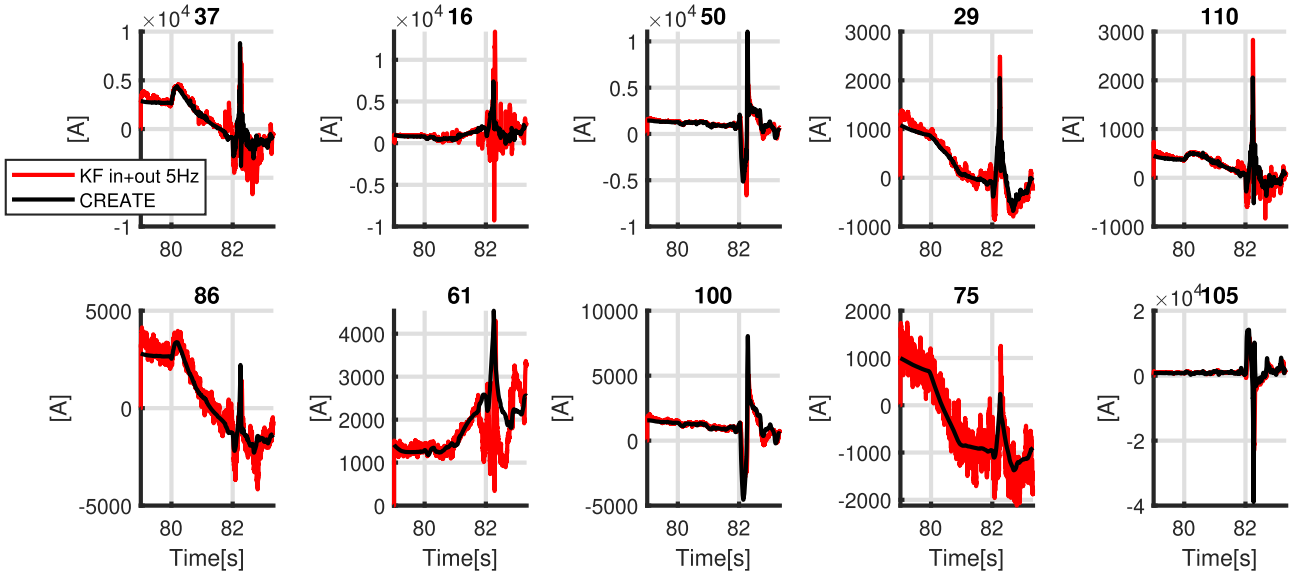

Figure 24. Comparison of eddy current on a selection of passive structures. The results obtained with the Kalman filter using in-vessel and out-vessel sensors are shown in red, while the black trace shows the simulated CREATE-L eddy currents.

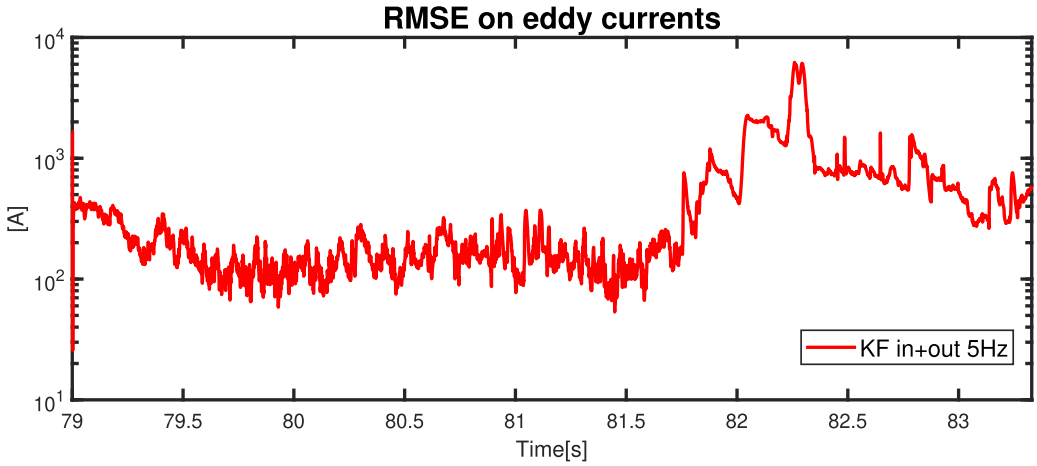

Figure 25. Root-mean-square error on the estimated currents in the 110 discretized passive conductors.

of the β_p and l_i parameters is significantly improved, as it can be seen from figures 16 and 17 (note that the module that estimates β_p and l_i is switched on when I_p reaches the value of 2 MA). Finally, in figure 18 the reconstruction of the passive currents induced in the selected structures highlighted in figure 6 is shown. It can be seen how the Kalman filter achieves convergence in about 2 s. The RMSE on all of the passive currents is also shown in figure 19

4.3. End of ramp-up and LH transition

In this segment, the plasma is in a diverted configuration, and the plasma current increases from 14.8 MA to 15 MA. This simulated scenario segment models a LH transition, with the value of β_p increasing from about 0.1 to 0.6. As for the previous cases, plasma boundary snapshots taken at the beginning, middle and end of the segment, together with the associated internal current density profiles are shown in figure 20.

The results obtained with P-EFIT with and without Kalman filter are compared in figures 21–25. For the case of the LH transition, the inclusion of the Kalman filter does not seem to provide any significant advantage in terms of equilibrium reconstruction accuracy, and the results are comparable to the ones obtained with the standard version of the code. In this case, the maximum value of the sum of the induced passive currents is about 165 kA, which is very small if compared to the value of the plasma current, two orders of magnitude larger. However, the eddy currents estimated by the Kalman filter match the simulated results obtained with CREATE-NL up to a satisfactory degree of accuracy, with some residual noise on the currents flowing in the outer-vessel structures.

4.4. End of flat-top and HL transition

The final segment presented in this section is a simulated HL transition at the beginning of the ramp-down phase. As in

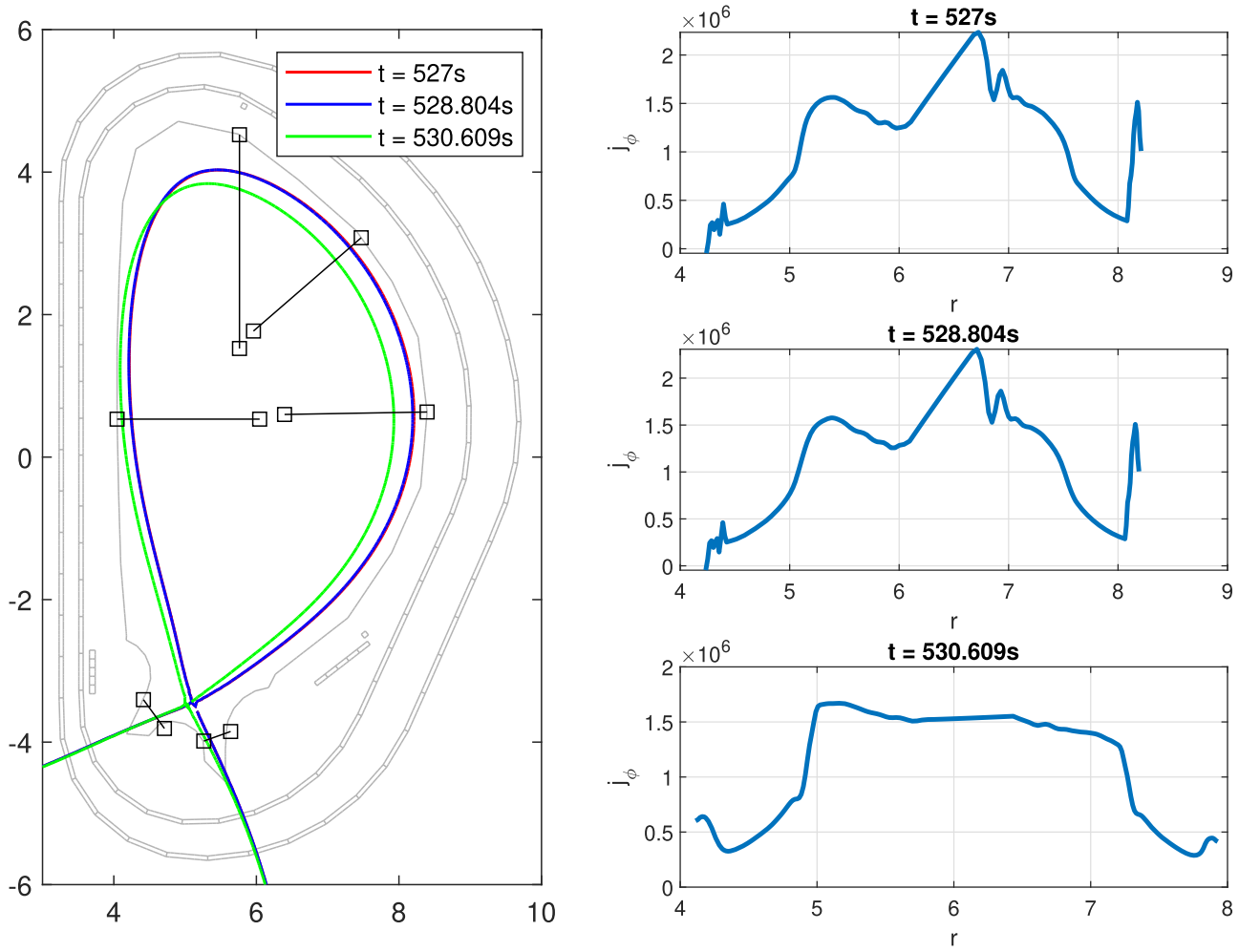

Figure 26. On the left, the plasma boundary at the initial, middle and final time instants of the considered segment. On the right, the internal plasma current density profiles associated to the same snapshots (taken along a horizontal line passing through the plasma centroid).

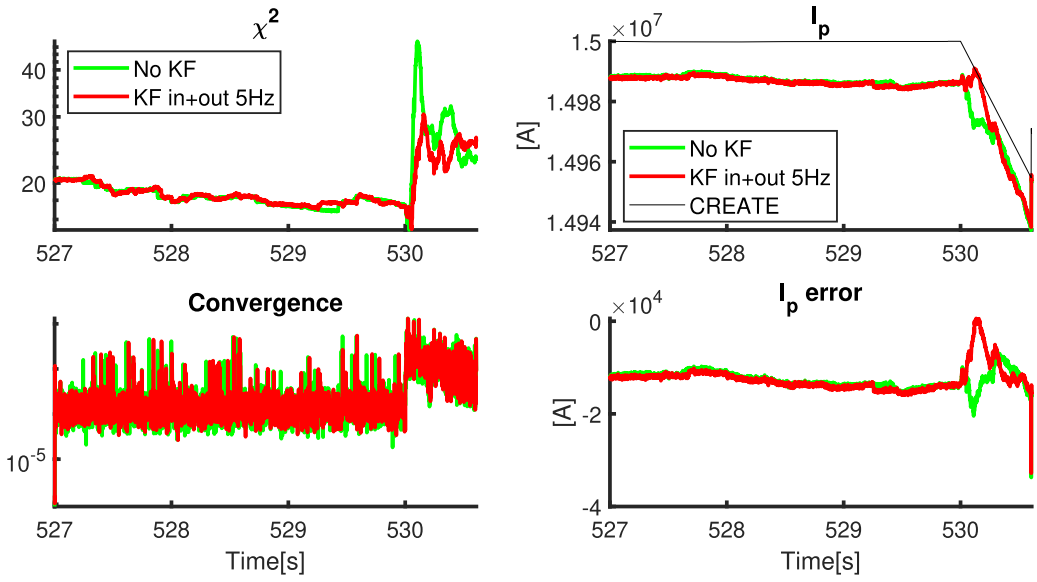

Figure 27. Magnetic reconstruction fitting χ^2, convergence and plasma current fitting (on a logarithmic scale). On the right, the plasma current fitting and fitting error.

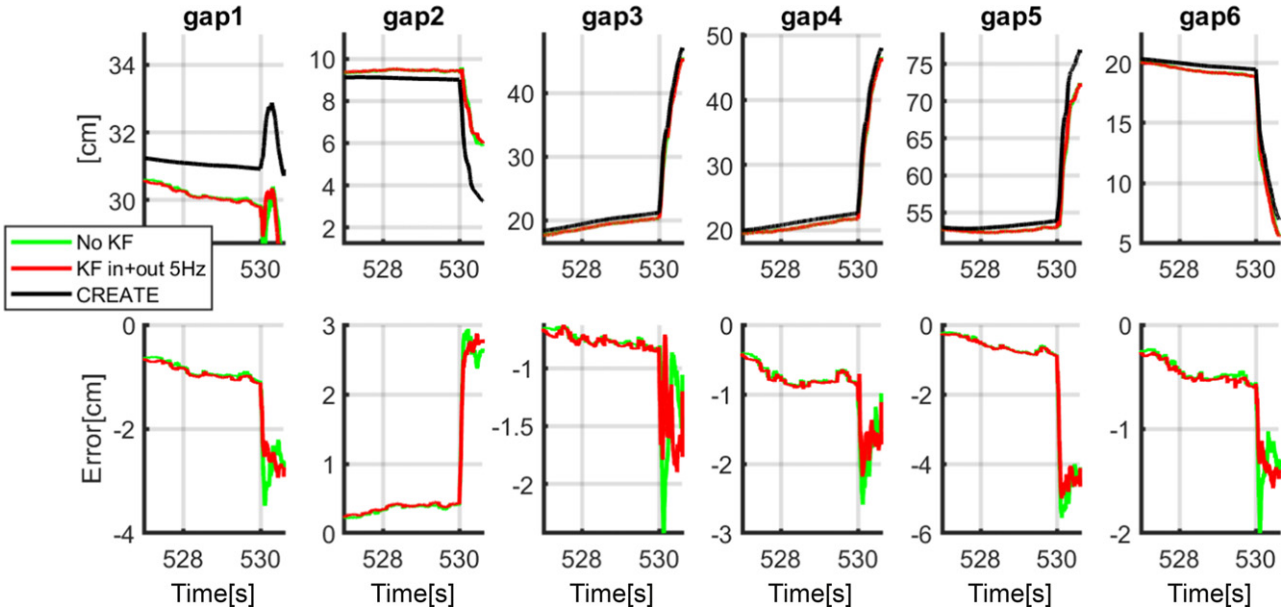

Figure 28. P-EFIT gap results (gaps #1 and #2 are not considered for limiter configurations). The black traces show the simulated gaps obtained with CREATE-L. The results obtained with the Kalman filter using in-vessel and out-vessel sensors are shown in red, while the green traces show the results without Kalman filter.

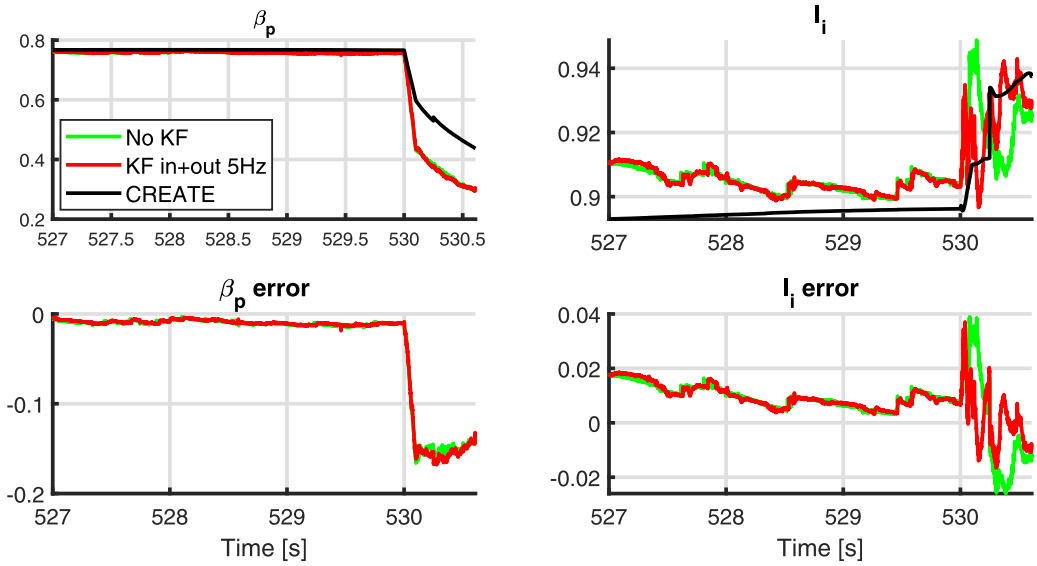

Figure 29. P-EFIT results in terms of the reconstruction of the β_p and l_i parameters. The results with Kalman filter using both in-vessel and out-vessel sensors are shown in red, while the green traces show the results when P-EFIT is run without the Kalman filter. The quantities simulated by CREATE-NL are shown in black.

the previous case, the plasma is in a diverted configuration, while this time the plasma current decreases from 15 MA to 14.95 MA. The value of β_p decreases from slightly less than 0.8 to about 0.3 in the terminal part of the segment, while the value of l_i undergoes a small increase, from 0.89 to 0.94. Plasma boundary snapshots taken at the beginning, middle and end of the segment, together with the associated internal current density profiles are shown in figure 26.

The results obtained with P-EFIT with and without Kalman filter are compared in figures 27–31.

As for the LH transition, also in the case of the HL one the results in terms of equilibrium reconstruction accuracy are comparable to the ones obtained with the standard version of the P-EFIT code; in this case, the χ^2 and the error on the estimated gaps, plasma current and on l_i is slightly reduced in the final part of the segment, as it can be seen from figures 27–29. In the first part of the segment, instead, the results of P-EFIT with and without the Kalman filter are practically equivalent, since the eddy currents are almost zero, as it can be seen from figure 30. The maximum value of the sum of the induced passive currents is very similar to that of the previous case, reaching 162 kA toward the end of the considered time window. The estimated passive currents match the simulated results obtained with CREATE-NL quite closely even in the most

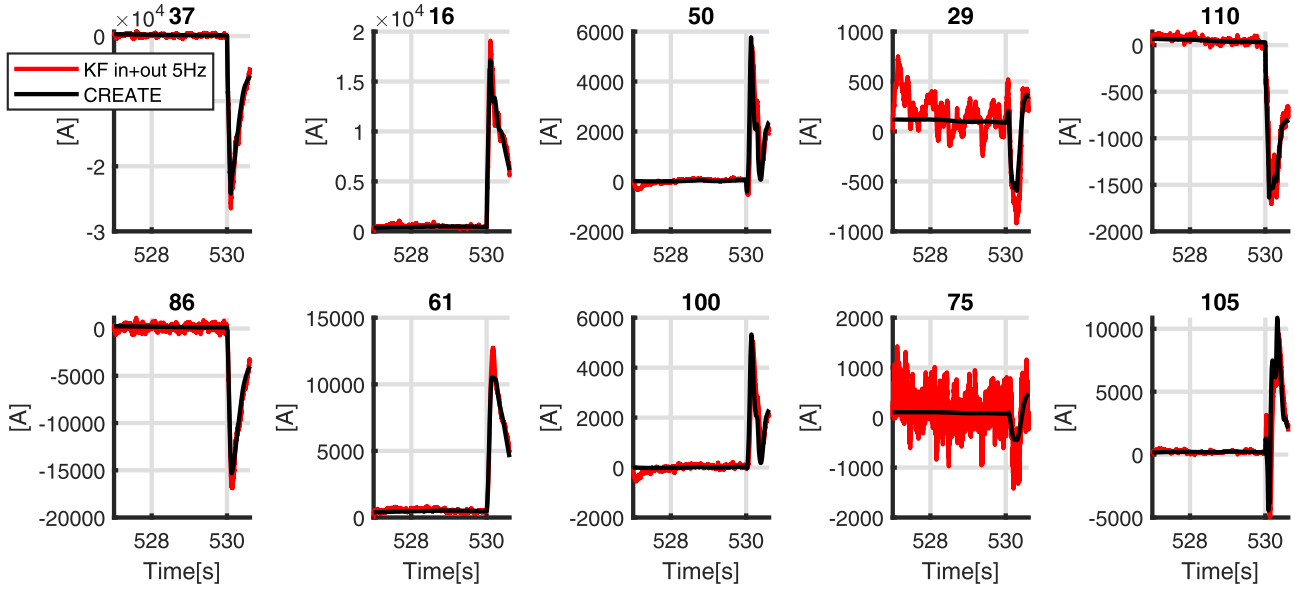

Figure 30. Comparison of eddy current on a selection of passive structures. The results obtained with the Kalman filter using in-vessel and out-vessel sensors are shown in red, while the black trace shows the simulated CREATE-L eddy currents.

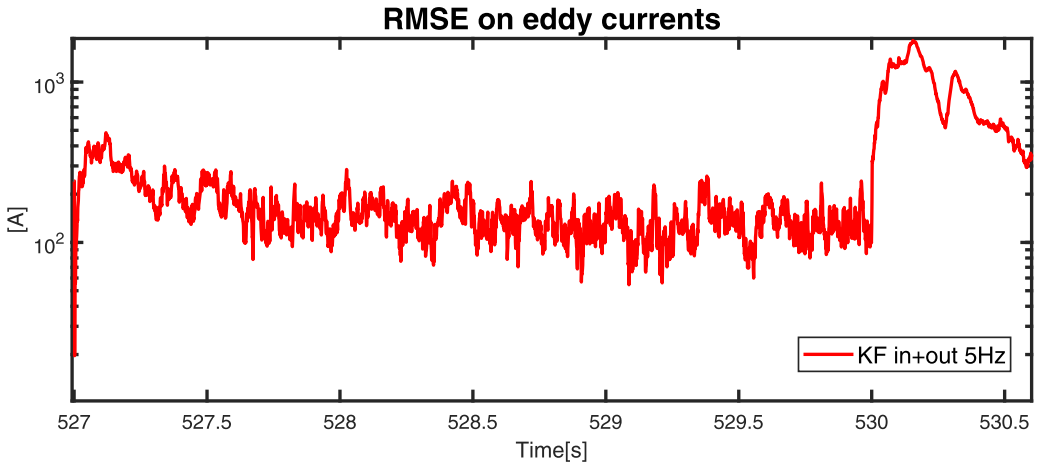

Figure 31. Root-mean-square error on the estimated currents in the 110 discretized passive conductors.

dynamical phases, again showing some residual noise on the currents flowing in the outer-vessel structures.

5. Conclusion

In this article, an observer based on the well-known Kalman filter, designed to estimate the induced currents on a discretized representation of the passive structures of a tokamak, has been presented. The proposed observer design is based on a vacuum model of the device, and the contribution due to the presence of the plasma is provided by the P-EFIT equilibrium reconstruction algorithm. Synthetic plasma discharges, simulated by means of the 2D code CREATE-NL, are used as a benchmark for the proposed approach, which shows good capabilities in estimating the induced currents. Numerical analyses indicate that low-pass filtering the active current measurements is crucial when implementing such an observer, as it greatly reduces the oscillations on the estimated passive currents. On the other hand, using only in-vessel measurements seems enough to achieve a good degree of accuracy, as the results do not significantly improve when additional, out-vessel measurements are added.

The inclusion of the proposed Kalman filter allows to achieve consistently better performance during highly dynamical ramp-up discharge phases, allowing a more reliable feedback control of the plasma shape, current and position and a better estimation of the considered plasma internal profiles integrals. On the other hand, the inclusion of the observer does not considerably improve the performance of the reconstruction algorithm in other delicate situations such as LH or HL transitions.

However, the availability of a reasonably accurate estimate of the passive currents could prove beneficial for different purposes then the mere equilibrium reconstruction. For instance, an estimate of the passive currents could also be useful to analyze the resulting forces on the conductive structures of

the tokamak. Another application example can be found in [38, 39], where a possible data-driven vertical stabilization system, based on the extremum-seeking technique described in [40], is proposed. This solution relies on an estimate of the plasma unstable mode, which is strongly dependent on the dynamics of the induced passive currents. To obtain that estimate, in [38, 39] a simplified state observer is designed on the basis of a plasma linearized model, under the assumption that the model-free nature of the extremum seeking algorithm is robust enough to compensate for the inevitable uncertainties arising from this gimmick. However, the availability of a proper estimate of the passive currents, such as the one proposed in the present work, could avoid the need for such a model, possibly leading to a completely model-free extremum-seeking based VS solution (with the exception of the vacuum model needed by the Kalman filter embedded in the equilibrium reconstruction code, which is fully linear and much easier to calibrate on plasmaless experiments).

It is also worth to remark that the adaptation of this observer to real-time operation does not prompt any particular difficulty; indeed, the execution time of the P-EFIT code is only loosely affected by the presence of the proposed observer. A real-time implementation of this solution is currently being pursued, in view of an experimental validation on the EAST tokamak.

Acknowledgments

This work has been funded by the Fusion For Energy Contract F4E-OPE0883. The work of Adriano Mele work has been carried out within the framework of the EUROfusion Consortium, funded by the European Union via the Euratom Research and Training Programme (Grant Agreement No. 101052200—EUROfusion). Views and opinions expressed are however those of the author(s) only and do not necessarily reflect those of the European Union or the European Commission. Neither the European Union nor the European Commission can be held responsible for them. This work was also partially supported by the Italian Research Ministry under the PRIN 20177BZMAH. The work of Yao Huang, Zhengping Luo, Bingjia Xiao and Qiping Yuan are also funded by the National MCF Energy R & D Program of China (No. 2018YFE0302100), the National Natural Science Foundation of China (Nos. 11805236 and 11875291).

ORCID iDs

Adriano Mele https://orcid.org/0000-0002-1782-858X
Zhengping Luo https://orcid.org/0000-0002-9560-6720
Massimiliano Mattei https://orcid.org/0000-0001-7951-6584
Alfredo Pironti https://orcid.org/0000-0003-4811-6232
Bingjia Xiao https://orcid.org/0000-0001-8692-2636
Qiping Yuan https://orcid.org/0000-0003-4292-1302

References

[1] Ariola M. and Pironti A. 2008 *Magnetic Control of Tokamak Plasmas* vol 187 (Berlin: Springer)
[2] Swain D.W. and Neilson G.H. 1982 An efficient technique for magnetic analysis of non-circular, high-beta tokamak equilibria *Nucl. Fusion* **22** 1015–30
[3] Ambrosino G., Celentano G., Garofalo F., Glielmo L. and Pironti A. 1992 On-line plasma shape identification via magnetic measurements *IEEE Trans. Magn.* **28** 1601–4
[4] Kurihara K. 2000 A new shape reproduction method based on the Cauchy-condition surface for real-time tokamak reactor control *Fusion Eng. Des.* **51–52** 1049–57
[5] Moret J.-M., Duval B.P., Le H.B., Coda S., Felici F. and Reimerdes H. 2015 Tokamak equilibrium reconstruction code LIUQE and its real time implementation *Fusion Eng. Des.* **91** 1–15
[6] Schneider W., McCarthy P.J., Lackner K., Gruber O., Behler K., Martin P. and Merkel R. 2000 ASDEX upgrade MHD equilibria reconstruction on distributed workstations *Fusion Eng. Des.* **48** 127–34
[7] Lao L.L., John H.S., Stambaugh R.D., Kellman A.G. and Pfeiffer W. 1985 Reconstruction of current profile parameters and plasma shapes in tokamaks *Nucl. Fusion* **25** 1611
[8] Appel L.C. *et al* 2006 A unified approach to equilibrium reconstruction *Proc. 33rd EPS Conf. Controlled Fusion and Plasma Physics* p P-2.160
[9] Ferron J.R., Walker M.L., Lao L.L., John H.E.S., Humphreys D.A. and Leuer J.A. 1998 Real time equilibrium reconstruction for tokamak discharge control *Nucl. Fusion* **38** 1055
[10] Huang Y., Xiao B.J., Luo Z.P., Yuan Q.P., Pei X.F. and Yue X.N. 2016 Implementation of GPU parallel equilibrium reconstruction for plasma control in EAST *Fusion Eng. Des.* **112** 1019–24
[11] Huang Y. *et al* 2020 GPU-optimized fast plasma equilibrium reconstruction in fine grids for real-time control and data analysis *Nucl. Fusion* **60** 076023
[12] Coccorese E., Morabito C. and Martone R. 1994 Identification of noncircular plasma equilibria using a neural network approach *Nucl. Fusion* **34** 1349
[13] Mele A., De Tommasi G., Mattei M. and Pironti A. 2020 A reduced basis approach to plasma equilibrium reconstruction in tokamaks *Fusion Eng. Des.* **154** 111520
[14] Lao L.L., John H.E.S., Peng Q., Ferron J.R., Strait E.J., Taylor T.S., Meyer W.H., Zhang C. and You K.I. 2005 MHD equilibrium reconstruction in the DIII-D tokamak *Fusion Sci. Technol.* **48** 968–77
[15] Qian J.P. *et al* 2016 EAST equilibrium current profile reconstruction using polarimeter–interferometer internal measurement constraints *Nucl. Fusion* **57** 036008
[16] Carpanese F. *et al* 2020 First demonstration of real-time kinetic equilibrium reconstruction on TCV by coupling LIUQE and raptor *Nucl. Fusion* **60** 066020
[17] Xing Z.A. *et al* 2021 Cake: consistent automatic kinetic equilibrium reconstruction *Fusion Eng. Des.* **163** 112163
[18] Jiang Y. *et al* 2021 Kinetic equilibrium reconstruction and the impact on stability analysis of KSTAR plasmas *Nucl. Fusion* **61** 116033
[19] Orsitto F.P. *et al* 2016 Diagnostics and control for the steady state and pulsed tokamak demo *Nucl. Fusion* **56** 026009
[20] Bettini P., Trevisan F. and Formisano A. 2002 An approach to the plasma magnetic contour identification in presence of eddy currents *IEEE Trans. Magn.* **38** 1089–92
[21] Pironti A. and Amato F. 1995 On-line plasma shape identification for use in control systems *Proc. 4th IEEE Conf. Control Applications* (Albany (USA))

[22] Mattei M., Pironti A. and Ambrosino R. 2013 H-infinity estimation of eddy currents in a tokamak *IFAC Proc. Vol.* **46** 33–8
[23] Berzak Hopkins L., Menard J., Majeski R., Lundberg D.P., Granstedt E., Jacobson C., Kaita R., Kozub T. and Zakharov L. 2012 Plasma equilibrium reconstructions in the lithium tokamak experiment *Nucl. Fusion* **52** 063025
[24] Hansen C., Boyle D.P., Schmitt J.C. and Majeski R. 2017 Equilibrium reconstruction with 3D eddy currents in the lithium tokamak experiment *Phys. Plasmas* **24** 042513
[25] Mele A., De Tommasi G., Pironti A. and Xiao B.J. 2018 Shape reconstruction and eddy current estimation via Kalman filter at the EAST tokamaks *45th EPS Conf. Plasma Physics (EPS2018)* (Prague: Czech Republic)
[26] Albanese R., Ambrosino R. and Mattei M. 2015 CREATE-NL+: a robust control-oriented free boundary dynamic plasma equilibrium solver *Fusion Eng. Des.* **96–97** 664–7
[27] Albanese R. and Villone F. 1998 The linearized CREATE-L plasma response model for the control of current, position and shape in tokamaks *Nucl. Fusion* **38** 723
[28] Albanese R. *et al* 2005 Design, implementation and test of the XSC extreme shape controller in jet *Fusion Eng. Des.* **74** 627–32
[29] Albanese R. *et al* 2011 Overview of modelling activities for plasma control upgrade in jet *Fusion Eng. Des.* **86** 1030–3
[30] Ariola M., Ambrosino G., Lister J.B., Pironti A., Villone F. and Vyas. P. 1999 A modern plasma controller tested on the tcv tokamak *Fusion Technol.* **36** 126–38
[31] Ambrosino R., Castaldo A., De Tommasi G., Luo Z.P., Huang Y., Mele A., Pironti A., Wang Y.H. and Xiao B.J. 2020 Model-based MIMI isoflux plasma shape control at the EAST tokamak: experimental results *2020 IEEE Conf. Control Technology and Applications (CCTA)* pp 770–5
[32] Mele A. *et al* 2019 MIMO shape control at the EAST tokamak: simulations and experiments *Fusion Eng. Des.* **146** 1282–5
[33] Castaldo A., Mele A., Albanese R., Ambrosino R., De Tommasi G., Luo Z.P., Pironti A., Xiao B.J. and Yuan Q.P. 2018 Simulation suite for plasma magnetic control at EAST tokamak *Fusion Eng. Des.* **133** 19–31
[34] Corona D. *et al* 2019 Plasma shape control assessment for JT-60SA using the create tools *Fusion Eng. Des.* **146** 1773–7
[35] Cruz N., De Tommasi G., Mattei M., Mele A., Miyata Y., Pironti A. and Suzuki T. 2017 Control-oriented tools for the design and validation of the JT-60SA magnetic control system *Control Eng. Pract.* **63** 81–90
[36] Giruzzi G. *et al* 2019 Advances in the physics studies for the JT-60SA tokamak exploitation and research plan *Plasma Phys. Control. Fusion* **62** 014009
[37] Vayakis G. *et al* 2012 Development of the ITER magnetic diagnostic set and specification *Rev. Sci. Instrum.* **83** 10D712
[38] De Tommasi G., Dubbioso S., Mele A. and Pironti A. 2021 Stabilizing elongated plasmas using extremum seeking: the ITER tokamak case study *2021 29th Mediterranean Conf. Control and Automation (MED)* pp 472–8
[39] De Tommasi G. *et al* 2022 Vertical stabilization of tokamak plasmas via extremum seeking (arXiv:2201.11708)
[40] Scheinker A. and Krstić M. 2017 *Model-free Stabilization by Extremum Seeking* (Berlin: Springer)